frontiers in Earth Science

ORIGINAL RESEARCH
published: 14 January 2020
doi: 10.3389/feart.2019.00343

Aeolian Remobilisation of the 2011-Cordón Caulle Tephra-Fallout Deposit: Example of an Important Process in the Life Cycle of Volcanic Ash

Lucia Dominguez[1], Costanza Bonadonna[1], Pablo Forte[2,3], Paul Antony Jarvis[1], Raffaello Cioni[4], Leonardo Mingari[5], Donaldo Bran[6] and Juan Esteban Panebianco[7]*

[1] Department of Earth Sciences, University of Geneva, Geneva, Switzerland, [2] Institute of Geosciences, Johannes Gutenberg University of Mainz, Mainz, Germany, [3] Departamento de Ciencias Geológicas, FCEN, Universidad de Buenos Aires, Buenos Aires, Argentina, [4] Department of Earth Sciences, School of Mathematical, Physical and Natural Sciences, University of Florence, Florence, Italy, [5] Barcelona Supercomputing Center, Barcelona, Spain, [6] Institute of National Agricultural Technology, San Carlos de Bariloche, Argentina, [7] The Institute of Earth and Environmental Sciences of La Pampa, National University of La Pampa (CONICET), Santa Rosa, Argentina

OPEN ACCESS

Edited by:
Roberto Sulpizio, University of Bari Aldo Moro, Italy

Reviewed by:
Claudio Scarpati, University of Naples Federico II, Italy
Ulrich Kueppers, Ludwig Maximilian University of Munich, Germany

***Correspondence:**
Lucia Dominguez
Lucia.Dominguez@unige.ch

Specialty section:
This article was submitted to Volcanology, a section of the journal Frontiers in Earth Science

Received: *21 July 2019*
Accepted: *10 December 2019*
Published: *14 January 2020*

Citation:
Dominguez L, Bonadonna C, Forte P, Jarvis PA, Cioni R, Mingari L, Bran D and Panebianco JE (2020) Aeolian Remobilisation of the 2011-Cordón Caulle Tephra-Fallout Deposit: Example of an Important Process in the Life Cycle of Volcanic Ash. Front. Earth Sci. 7:343. doi: 10.3389/feart.2019.00343

Although volcanic eruptions represent short periods in the whole history of a volcano, the large amount of loose pyroclastic material produced, combined with aeolian processes, can lead to continuous, long-lasting reworking of volcanic products. Driven by wind, these processes significantly influence the geomorphology and prolong the impacts of eruptions on exposed communities and ecosystems. Since such phenomena are of interest to scientists from a range of disciplines (e.g., volcanology, atmospheric and soil sciences), a well-defined, common nomenclature is necessary to optimise the multidisciplinary characterisation of both processes and deposits. We, therefore, first describe ash wind-remobilisation processes and provide definitions for appropriate terms consistent with the World Meteorological Organisation's (WMO's) classification of lithometeors. Second, we apply these definitions to investigate aeolian remobilisation of the 2011 Cordón Caulle (Chile) tephra-fallout deposit, which has strongly impacted rural communities in the Argentinian Patagonia steppe. We combine field observations and a physical characterisation of systematically collected ground and airborne material in order to identify the secondary deposits associated with: (i) non-erodible surface roughness elements (e.g., vegetation and rocks) and (ii) pre-existing mounds or similar erodible bedforms. Grainsize analysis shows that wind-remobilised particles have a specific size range, from <0.4 to 500 μm, with a 95% of the material between 1 and 255 μm, median values of 25–135 μm and modes of 30–95 μm. We find that 15–40% of the remobilised material ranges from 63–125 μm, coinciding with the size range which minimises the wind threshold friction velocity. Interestingly, particle shape analysis shows that for this size fraction, remobilised particles display the largest differences in shape descriptors (convexity, solidity and circularity) with respect to the primary ash, indicating abrasion and rounding due to saltation. Although particle (size and shape) and

deposit features (morphology and structures) alone are insufficient to interpret transport mechanisms, their combination suggests that whilst saltation is the most common particle transport mechanism, suspension and creep also play an important role. As well as inferring transport mechanisms from this combined approach, we also demonstrate how the correlation of the primary volcanic source with the associated remobilised deposits is fundamental to our understanding of the life cycle of volcanic ash.

Keywords: tephra fallout, wind remobilisation, transport and deposition processes, lithometeor classification, volcanic ash life cycle

INTRODUCTION

Although volcanic eruptions are often short lived and represent discrete time windows within the whole history of a volcano, the life cycle of volcanic ash is a continuous process due to the action of erosive processes (e.g., remobilisation by wind and/or water) on a large amount of loose volcanic material produced by explosive eruptions (Cas and Wright, 1987).

Studies of recent eruptions [e.g., Katmai 1902, Alaska; Eyjafjallajökull 2010, Iceland; Hudson 1991, Cordón Caulle (CC) 2011 and Calbuco 2015, Chile] have demonstrated that syn- and post-eruptive aeolian remobilisation of volcanic ash exacerbates the impact of primary tephra fallout, and extends it to larger areas over prolonged periods of time (Bitschene, 1995; Hadley et al., 2004; Wilson et al., 2011; Thorsteinsson et al., 2012; Elissondo et al., 2016; Reckziegel et al., 2016; Forte et al., 2018). The associated impacts have been summarised in the recent Global Assessment Report of the United Nation Office for Disaster Risk Reduction (Jenkins et al., 2015). One of the most relevant impacts concerns public health since long-term exposure to high concentrations of respirable particles (i.e., diameter $\leq$10 μm, known as PM10) can trigger or aggravate respiratory and ophthalmological diseases (Hincks et al., 2006; Baxter and Horwell, 2015; Carlsen et al., 2015). Significant disruption can also occur to critical infrastructures such as roads due to reduced visibility and traction, power systems due to ash clogging or air traffic due to high atmospheric ash concentration (Hadley et al., 2004; Wilson et al., 2013; Jenkins et al., 2015; Craig et al., 2016), whilst the agriculture sector is strongly affected due to animal starvation, abrasion and soil erosion (Wilson et al., 2011; Fernández-Arhex et al., 2013; Craig et al., 2016; Forte et al., 2018). wind-remobilisation of fine ash also has a significant environmental effect by increasing droughts in source regions and enhancing precipitations in distal areas (Langmann, 2013; UNEP et al., 2016).

Wind erosion processes of volcanic material have been studied through two main approaches: (i) a volcanological approach and (ii) a soil-erosion and atmospheric approach. Volcanological studies of aeolian ash remobilisation primarily focus on associated impacts (Bitschene, 1995; Hincks et al., 2006; Wilson et al., 2011; Carlsen et al., 2015; Forte et al., 2018) or the characterisation of both the associated deposits (Hobbs et al., 1983; Liu et al., 2014; Miwa et al., 2018) and the physical processes through laboratory experiments (Douillet et al., 2014; Del Bello et al., 2018) and numerical modelling (Barsotti et al., 2010; Leadbetter et al., 2012; Folch et al., 2014; Reckziegel et al., 2016; Mingari et al., 2017). Despite this significant effort, no studies have yet correlated wind transport with deposition processes of loose volcanic particles. In the field of soil erosion and atmospheric science, wind-induced phenomena are commonly associated with mineral dust and sand erosion processes, regardless of the primary particles' source (Hadley et al., 2004; Thorsteinsson et al., 2012; Arnalds et al., 2013; Panebianco et al., 2017). These studies have mainly focussed on the dependence of atmospheric particulate concentration on meteorological and surface conditions and do not investigate the relationships with the primary tephra fallout deposits and the variation in the surface cover due to the dynamic secondary ash deposition. A first attempt to converge understanding of both mineral dust erosion and wind remobilisation of volcanic ash was undertaken by Langmann (2013), who compared the emission, atmospheric load and deposition of mineral dust versus volcanic ash.

There is a clear need for a strong collaborative and multi-disciplinary approach to improve our understanding of wind-remobilisation of volcanic particles and support risk reduction strategies including numerical forecasts and the implementation of mitigation measures. One of the main challenges is the lack of common terminology and definitions. The main objectives of this paper are to: (i) correlate volcanological terms used to describe wind-remobilisation of volcanic ash with atmospheric definitions of aeolian phenomena, mostly developed by the World Meteorological Organisation (WMO); (ii) describe depositional features of ash remobilised by these phenomena, using the 2011-CC eruption, Chile, primary tephra fallout as a case study and (iii) characterise aeolian transport and deposition mechanisms of CC ash according to the size and shape of particles combined with field observations. Primary deposit refers here to the deposition of pyroclasts generated by explosive eruption, whilst wind remobilisation implies syn- or post-eruptive reworking transport of freshly erupted volcanic particles. These processes are different from long-term physical and/or chemical weathering which are associated with epiclastic deposits (Fisher and Schmincke, 1984; Cas and Wright, 1987).

TERMINOLOGY

Previous Studies

Although the importance of remobilisation of pyroclastic material has been recognised for the last few decades

(Fisher and Schmincke, 1984; Cas and Wright, 1987; Mcphie et al., 1993), such processes only became of interest after the 1991 eruption of Hudson volcano, Chile. Remobilisation here was first defined as *ash storm* by Bitschene (1995) whilst several authors have since described the process using different terms with no clear distinction between phenomena, transport, deposition and deposits. Typically, the term 'ash storm' was adopted to describe events of intense and persistent winds generating massive remobilisation of fresh volcanic deposits (Wilson et al., 2011; Thorsteinsson et al., 2012; Forte et al., 2018). Liu et al. (2014) distinguished between extreme events, *ash storms* (öskubylar in Icelandic), and low-intensity events, *ash mists* (öskumistur), both with high potential to reduce visibility. Modelling studies of ash dispersal refer to the suspension of fine ash into the atmosphere as *ash resuspension*, *remobilisation of volcanic ash, relic volcanic ash* or *dust storms* (Barsotti et al., 2010; Leadbetter et al., 2012; Bagnato et al., 2013; Folch et al., 2014; Ulke et al., 2016; Mingari et al., 2017). Forte et al. (2018) introduced the term *ash devil* to describe local and short duration whirlwinds that were often observed after the 2011 CC eruption, whilst Mingari et al. (2017) used the term *windblown dust* in a modelling study of ancient pyroclastic material resuspension. This term was already used by Cas and Wright (1987) to group the two transport mechanisms, traction and suspension, in which air is the essential interstitial medium.

Wind-Remobilisation Phenomena

According to the Atlas of the WMO (WMO, 1975), a *lithometeor* is an ensemble of mostly solid particles in the atmosphere. A classification of lithometeors is summarised in **Table 1** (WMO, 1975). There are two main types of lithometeors classes: particles already *suspended* in the atmosphere and those being *lifted* or *raised* from the ground by the wind (drifting and blowing). Suspended particles are associated with dust events that occurred prior to the time of observation whereas raised-particle phenomena concern particles locally raised by a sufficiently strong wind at the time of observation. Atmospheric conditions (e.g., wind intensity, turbulence) and soil conditions (e.g., moisture, grainsize, particle density), control the transitions between drifting, blowing and dust/ash storms and consequently the height to which particles are lifted. Based on the WMO protocol, these lithometeors are associated with four categories of visibility loss (Shao, 2008), where visibility is reduced to: 10 km (dust haze), 10–1 km (blowing dust), 1 km–200 m (dust storm) and <200 m (severe dust storm) (**Table 1**). A more detailed summary with examples is presented in **Supplementary Figure S1**.

The WMO classification (**Table 1**) is also applicable to volcanic particles, as shown in **Figure 1**. The terms 'dust' and 'sand', which refer to rock-derived, solid, inorganic particles of <63 and 63 μm to 2 mm, respectively (UNEP et al., 2016), can be used to describe volcanic ash (<2 mm) and are the equivalent of fine and coarse ash, respectively. In fact, Butwin et al. (2019) compiled various dust and ash phenomena in Iceland, that were previously classified as haze, dust storms, sandstorms and dust whirls, by applying the WMO classification.

Wind-Transport Mechanisms

Wind erosion results from the balance between aerodynamic forces, that remove particles from the surface, and resistive forces, such as gravity and inter-particle cohesion (Shao and Lu, 2000). The wind friction velocity u^*, a function of meteorological conditions, determines the capacity of the wind to remobilise particles whilst the threshold friction velocity u^*_t, defined as the minimum friction velocity required to initiate the motion, depends on the physical soil properties (e.g., grainsize, density, aggregation, shape of particles) and surface conditions (e.g., soil moisture, roughness elements) (Shao, 2008). For typical aeolian conditions, u^*_t is smallest for particles of 75–100 μm (very fine sand) (Kok et al., 2012).

Once motion is initiated, particles can be transported through three main mechanisms: *suspension*, *saltation* or *creep*, depending on the grainsize, particle density and wind conditions (Bagnold, 1941; Pye, 1987; Shao and Lu, 2000; Shao, 2008; Kok et al., 2012). As wind velocity increases, very fine sand-sized particles with the smallest u^*_t are the first to move by *saltating* close to the surface (Shao and Lu, 2000). The impact of these particles on the bed drives the ejection of other particles, which can either be entrained into the atmosphere by suspension or mobilised by creeping across the surface. Wind typically cannot lift smaller particles (<70 μm) by direct action of aerodynamic forces because of their strong cohesive forces. Once ejected by saltators, smaller particles enter into a short-term (∼20–70 μm) or long-term (<20 μm) *suspension*. Particles suspended in the long term can remain in the atmosphere for up to several weeks and travel thousands of kilometres from the source (Kok et al., 2012). Particles larger than 500 μm normally cannot saltate and therefore usually move by *creep* (reptation or rolling).

Deposition Mechanisms and Associated Deposits

Deposition of remobilised particles occurs either through dry or wet deposition. Dry deposition results from gravitational settling in roughness elements that act as sediment traps, e.g., vegetation canopies (Kok et al., 2012). Wet deposition occurs when particles serve as nuclei for water or ice precipitation and subsequently grow and settle (Langmann, 2013). The morphology and structure of dry deposits are controlled by the wind directionality and flow regime, transport mechanisms, material availability and topography (Bagnold, 1941). Deposition, strongly dependent on particle concentration and both fluid and particle properties, normally occurs when the flow decelerates and particles settle down by gravity. Depending on the type of transport processes, resulting deposits are characterised by a suite of features that are key for distinguishing between primary and remobilised deposits (Cas and Wright, 1987; Mcphie et al., 1993), such as composition, geometry, bedding, grainsize and particle sorting (**Table 2**). Remobilised deposits, composed of a mixture of fresh material, old volcaniclastic sediments and no-volcanic material, display geometric differences with respect to the primary tephra deposits. Whilst primary deposits typically thin with distance from the vent, remobilised deposits contain local lateral discontinuities in thickness which can vary over time.

TABLE 1 | Lithometeors classification according to the World Meteorological Office (WMO, 1975).

Mechanism	Phenomenon	Definition	Visibility[1] loss categories
Suspension of particles in the atmosphere	Haze	A suspension in the air of extremely small, dry particles invisible to the naked eye and sufficiently numerous to give the air an opalescent appearance.	
	Dust haze	A suspension in the air of dust or small sand particles, raised from the ground prior to the time of observation by a dust storm or sandstorm. The dust storm or sandstorm may have occurred either at or near the observation site or far from it.	Dust haze, consists of aeolian dust particles homogeneously suspended in the atmosphere. These are not actively entrained, but have been uplifted from the ground by a dust event that occurred prior to the time of observation or from a considerable distance. Visibility may sometimes be reduced to 10 km.
	Smoke	A suspension in the air of small particles produced by combustion.	
Drifting or blowing of particles *raised* by the wind	Drifting dust or sand	Dust or sand raised by the wind to small heights above the ground. The visibility is not sensibly diminished at eye level (1.80 m above the ground).	
	Blowing dust/sand	Dust or sand raised by the wind to moderate heights above the ground. The horizontal visibility at eye level is sensibly reduced (1.80 m above the ground).	Blowing dust is the state where dust is transported locally by strong winds at the time of observation reducing visibility to 1–10 km.
	Dust storm or sandstorm	An ensemble of particles of dust or sand energetically lifted to great heights by a strong and turbulent wind.	A dust storm is the result of strong turbulent winds entraining large quantities of dust particles, reducing visibility to between 200 m and 1 km. A severe dust storm is characterised by very strong winds that lift up large quantities of dust particles, reducing visibility to less than 200 m.
	Dust/sand whirl (dust devil)	An ensemble of particles of dust or sand, sometimes accompanied by small litter, raised from the ground in the form of a whirling column of varying height with a small diameter and an approximately vertical axis.	

[1] *Based on the WMO protocol, Shao (2008) proposed 4 four visibility categories of dust events. Visibility, for aeronautical purposes, is defined as the maximum of either the "greatest distance at which a black object of suitable dimensions, situated near the ground, can be seen and recognised when observed against a bright background" or "the greatest distance at which lights in the vicinity of 1000 candelas can be seen and identified against an unlit background" (ICAO, 2007). Definitions directly from https://cloudatlas.wmo.int/.*

Additionally, unsteady wind conditions generate cross-bedding structures which are not present in primary tephra deposits (Bagnold, 1941; Mcphie et al., 1993). Grainsize and sorting in remobilised deposits are directly related to the wind capacity for removing and sorting particles from the ground and to the local conditions at deposition, whilst in primary deposits they mostly depend on the magmatic fragmentation efficiency, fractionation during transport in the plume (Cas and Wright, 1987) and size-selective sedimentation processes (e.g., particle aggregation, gravitational instabilities).

2011 CORDÓN CAULLE ERUPTION: PRIMARY TEPHRA-FALLOUT DEPOSIT

The Puyehue-CC is a late Pleistocene to Holocene volcanic complex system located in the Southern Volcanic Zone of the Central Andes in Chile. This basaltic-to-rhyolitic system constitutes the Puyehue stratovolcano and the CC fissure complex. Three major eruptions [volcanic explosivity index (VEI) > 3] in the last 100 years (1921–22, 1960 and 2011) have been associated with the CC rift zone (Global Volcanism Program, 2013). The most recent, starting the 4th June 2011, was a long-lasting rhyolitic eruption classified as VEI 4-5 (Bonadonna et al., 2015). Plumes with heights between ca. 3–14 km above the vent, generated approximately 1 km^3 DRE of tephra-fallout deposit that, due to the prevailing winds, extended toward the Argentinian Andes and Patagonian steppe. The combination of a long-lasting eruption and strong, shifting winds resulted in a complex primary tephra-fallout sequence of deposits over a wide area (Collini et al., 2013; Bonadonna et al., 2015; Pistolesi et al., 2015). The primary tephra-fallout deposit consists of four main units containing 13 layers (**Figure 2A**). Unit I (layers A to F), originated from the climactic phase of the eruption (4–5 June) with plumes of 11–14 km above sea level, was dispersed to the SE and produced a lapilli-bearing bed of total volume ca. 0.75 km^3 (Pistolesi et al., 2015). The second phase, with plumes of 8–12 km a.s.l., dispersed briefly to the N and then SE, depositing the lapilli-bearing Unit II (layers G and H). Unit III, deposited from plumes of fluctuating height and dispersed mainly to the E-ESE during the 6–15 June, is composed of five layers (K1–K5) mainly fine-grained except for the coarser (fine-lapilli) layer K2. In distal areas (about 300 km east from the vent), layers K1–K5 are fine-grained and not clearly distinguishable. Unit IV, deposited after 15 June, is a millimetres-thick fine ash deposit only found very proximally (<20 km from the vent) and represents the end of the explosive phase of the eruption (Pistolesi et al., 2015).

A wide area in Argentina (>100,000 km^2) was affected by tephra dispersion and sedimentation throughout the eruption (Wilson et al., 2013; Craig et al., 2016; Elissondo et al., 2016;

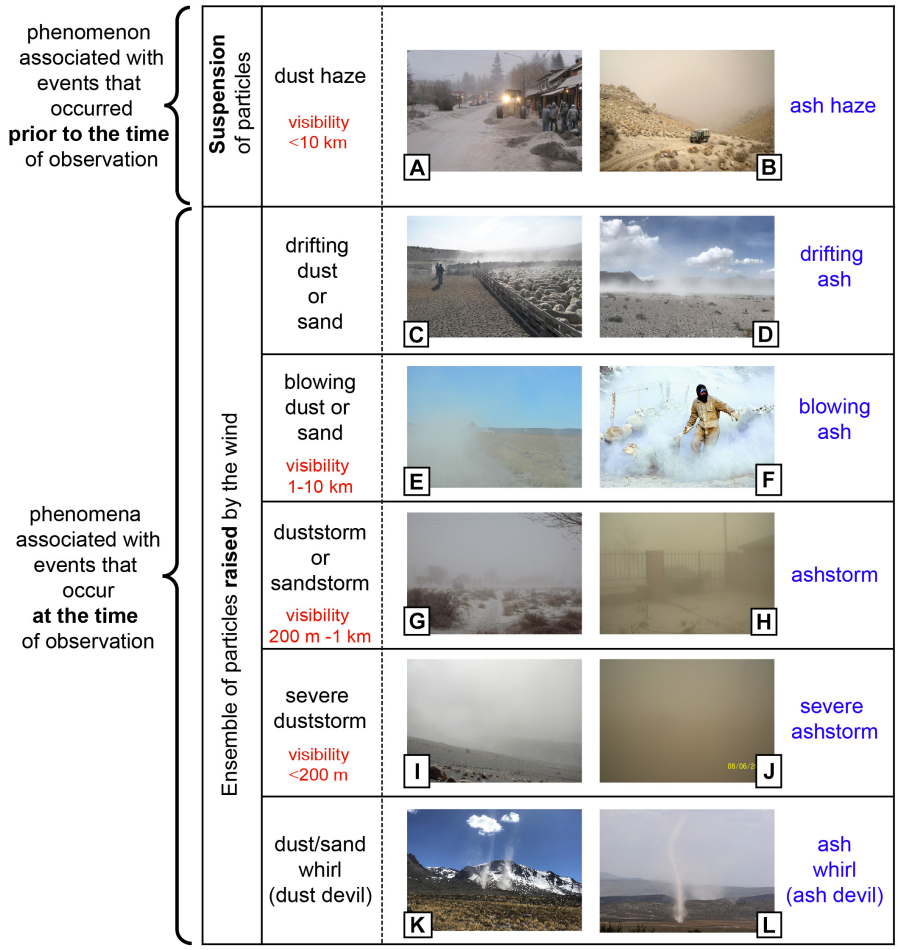

FIGURE 1 | Correspondence between wind-remobilisation of volcanic ash (right column) and the WMO classification for lithometeors (left column). Also see **Table 1** for further details. **(A–C,E–H,J,L)** Photographs taken in or nearby Ingeniero Jacobacci (Argentina), 230 km from the CC vent. **(D,I,K)** Photographs taken around Sabancaya volcano (Peru), about 5 km from the vent. Source of photographs: **A,B,G,H**, Radio Nacional de Jacobacci LRA54; **C,F**, Jazmin Miguel; **D,E,K**, Lucia Dominguez; **I**, Paul A. Jarvis; **J**, Gonzalo Pozos; **L**, Donaldo Bran.

Forte et al., 2018). As with the 1991 Hudson eruption, one of the most important long-term consequences has been the remobilisation of ash, particularly in the arid and semi-arid regions of the Patagonian steppe (Wilson et al., 2011). Whilst the three main phases of the eruption lasted only a few days, remobilisation continues up to the time of writing (2019).

Field observations suggest that the primary Unit III is the most susceptible to remobilisation. **Figure 2B** shows the isopach map of Unit III based on the data reported in Gaitán et al. (2011) and Pistolesi et al. (2015), combined with satellite images (MODIS Terra-Aqua and Landsat).

MATERIALS AND METHODS

Data Collection

In order to characterise remobilisation of the CC tephra-fallout deposits, two strategies of data collection were implemented. First, field observations, from a 2016 campaign, were made along an NNW-SEE transect from the Paso Samoré (Chile-Argentina border), through Villa La Angostura (VLA) in the Andes; San Carlos de Bariloche (SCB); Pilcaniyeu (PC) to Ingeniero Jacobacci (IJ) in the Patagonian steppe (**Figures 2B**, **3A**), and were integrated with previous descriptions of the primary tephra-fallout deposit made by Bonadonna et al. (2015) and Pistolesi et al. (2015). A total of 56 ground samples were collected along this transect (**Figure 2B**, ground). Second, samples from the syn-deposition collection of remobilised airborne material, implemented by the National Institute of Agricultural Technology of Argentina (INTA) since 2011, were analysed. This collection was carried out using dedicated clusters of horizontal sample collection located in seven strategic erosion sites (**Figure 2B**, airborne), each consisting of three collectors at fixed heights (0.15, 0.5 and 1.5 m; **Figure 2C**). Four of the seven clusters, where maximum mass fluxes have been recorded, were selected for this study (sites S2, S3, S4 and S6; **Figure 2B**) accounting for about 50 samples of a total of 170 periodically collected

TABLE 2 | Summary of distinctive features of primary tephra-fallout versus wind ash-remobilisation deposits.

Deposit feature	Primary tephra-fallout deposit	Wind ash-remobilisation deposit
Local thickness variability	Locally homogenous thickness	Large thickness variability in time and space (also at a very short-scale), depending on wind intensity, vegetation cover and topography.
Downwind thinning	Thickness typically decreases with distance from the vent. Secondary maxima in thickness can be present due to complex sedimentation processes (e.g., aggregation, gravitational instabilities).	No regular variation with the distance from the vent. Possible local thickening related to wind pattern and superficial features (i.e., topography, vegetation).
Local sorting	Mostly related to the interplay between atmospheric transport and size-selective sedimentation processes (e.g., aggregation, gravitational instabilities). Sorting poorly variable at the local scale.	Variable sorting at a local scale, controlled by surface wind velocity and surface soil features.
Local grainsize	Local grain size distribution dependent on original total grain size distribution and atmospheric transport and sedimentation processes (e.g., aggregation, gravitational instabilities).	
Bedding	Typically planar beds. Deposit can be either massive or stratified depending on eruption dynamics. Possible presence of vertical grain size grading.	Presence of short-wavelength cross-bedding, related to unsteady wind conditions and sustainment of remobilised ash by wind. Presence of lenticular bedding.
Composition	Juvenile (fresh magma, crystals) and non-juvenile fragments.	Mixture of fresh and/or old volcaniclastic material and/or sediments.
Shape of particles	Mainly related to magma rheology and amount, size and shapes of vesicles.	Primary shape modified by grain-grain or grain-substratum interaction during transport. Fine material possibly produced by abrasion. Presence of exotic fragments (from pre-existing loose sediments) recognisable from the shape (highly rounded).

since 2011 to 2015 by INTA. Based on this sampling, Panebianco et al. (2017) provide a detailed discussion of the sediment mass flux and their dependence on the landscape geomorphology, material availability and vegetation cover. In this study, we combine ground and airborne sampling to investigate the relationship between the transport and deposition mechanisms of remobilised ash and the primary tephra fallout.

Analyses

All samples were manually dry sieved at half-ϕ intervals down to a size of 1ϕ (500 μm). Finer material was analysed with a laser–diffraction, particle size analyser (CILAS 1180) at the University of Geneva. Shape distribution parameters (median grainsize Md_ϕ and sorting α_ϕ) were calculated according to Inman (1952).

For shape analysis, 12 samples were selected for sieving to finer fractions (class 1: $>$ 4ϕ or $<$ 63 μm, class 2: 4ϕ–3ϕ or 63–125 μm, class 3: $<$ 3ϕ or $>$ 125 μm) before backscatter electron images were captured by a Jeol JSM scanning electron microscope (SEM) at the University of Geneva. Binary images obtained from the SEM images were analysed by using the macro proposed by Liu et al. (2015) to calculate solidity, convexity and circularity, these being the most used shape descriptors because of their usefulness in the interpretation (Liu et al., 2015). Solidity, the ratio between the areas of the particle and its convex hull, represents a measure of morphological roughness, while convexity, the ratio between the convex hull and particle perimeter, describes textural roughness at the particle surface. Circularity, also known as form factor or Cox circularity, describes the general roundness of particles. For the purpose of this study, values of convexity, close to one indicate abrasion of small irregularities, whilst similar values of solidity and circularity show more roundness toward spherical shapes.

Particle density, taken as the skeletal density without open vesicularity, has been measured using a helium pycnometer at the University of Geneva. The average density of remobilised particles is 2419 ± 0.03 kg m^{-3}, value within the average density of primary tephra-fallout particles in the proximal ($<$100 km from the vent) and distal ($\sim$300 km from the vent) areas which is 2395 ± 0.06 and 2493 ± 0.02 kg m^{-3}, respectively.

RESULTS

Field Observations of Ash-Remobilised Deposits

Field observations along the NNW-SSE transect suggest that the primary tephra-fallout deposit is better preserved proximally rather than in distal areas, particularly for the coarser-grained Units I and II. In contrast, it is noticeable all along the transect that the fine ash of Unit III has been transported and redistributed by wind (**Figure 3**). The best-preserved primary outcrops of Unit III are located in either rain-forested, proximal areas (e.g., close to Paso Samoré or VLA, **Figure 3B**) or in the small valleys dissecting the typical wetlands in the region of PC, known as *mallines* (**Figure 3B**). Although scarce, evidence of remobilisation in proximal areas occurs mainly on mountain tops where vegetation is absent or rare (**Figure 3B**, VLA). Unit III has undergone reworking both proximally and distally, displaying localised variations in thickness and aeolian structures (e.g., cross-stratification structures). The local variations in deposit thickness are strongly dependent on the surrounding vegetation and topography. We find that in some proximal areas, the

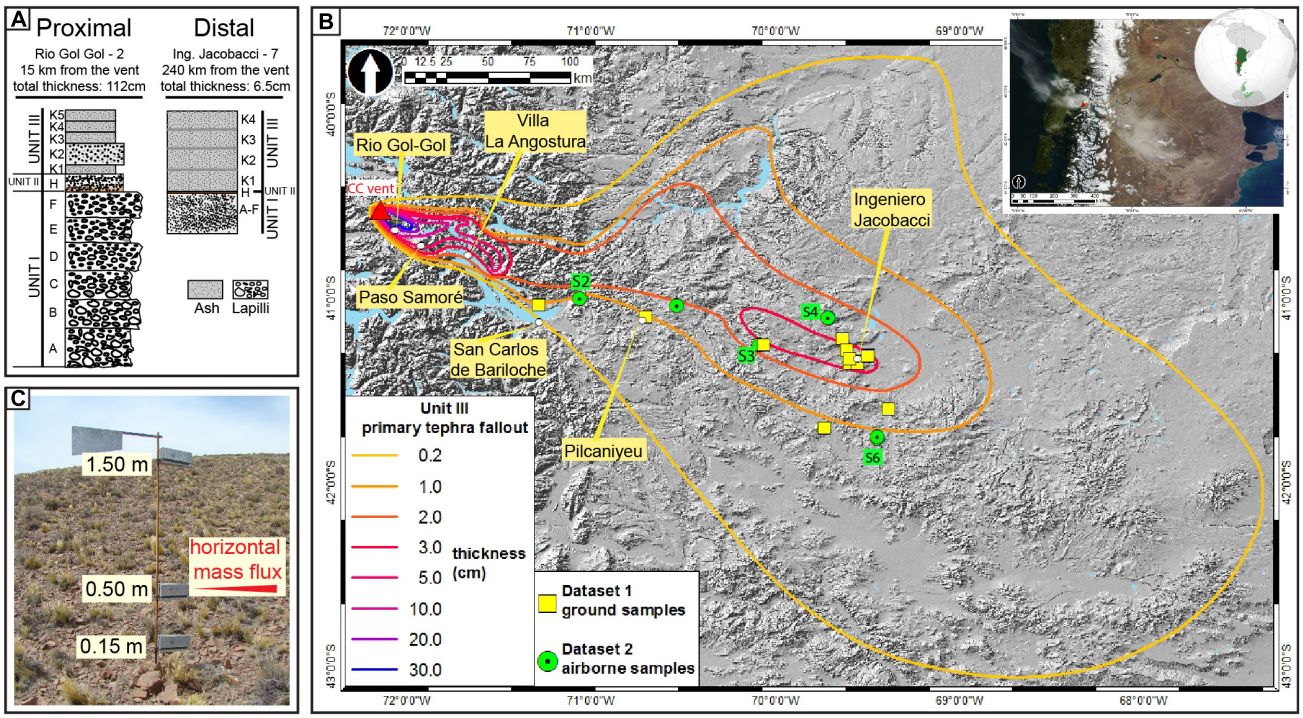

FIGURE 2 | (A) Stratigraphy associated with the 2011-Cordón Caulle primary tephra-fallout deposit showing a typical section in the proximal areas (i.e., Rio Gol-Gol, 15 km from the vent) and in the distal areas (i.e., Ingeniero Jacobacci, 240 km from the vent) (Pistolesi et al., 2015). **(B)** Isopach map of Unit III in cm. Sampling location of ground (i.e., Dataset 1) and airborne (i.e., Dataset 2) samples is shown. Selected sites for airborne material (i.e., Dataset 2) correspond to sites S2, S3, S4 and S6. Satellite image (MODIS-Aqua), January 2013 (top right corner) (Source: https://earthobservatory.nasa.gov/). **(C)** Dust-sampler vertical pole with a wind-oriented weather vane designed to collect at least 86% of the remobilised material crossing a horizontal flow through an opening of 10 cm^2 (more details in Panebianco et al., 2017).

thickness of Unit III has locally increased by a factor of two since the study of Pistolesi et al. (2015) (**Figures 3C,D** Paso Samoré, VLA), whilst in distal areas these variations become more pronounced, varying from 1 to 40 cm (**Figures 3C,D**, CO, IJ).

Greater ash remobilisation in distal areas with respect to proximal/medial areas is compatible with an increased availability of ash, as indicated by the secondary thickness maximum of Unit III (**Figure 2B**), with a wider dispersal area typical of distal areas and with the arid steppe climate. In fact, there is a climate gradient with significantly contrasting annual precipitations between the Andes Range (800–2500 mm $year^{-1}$) and the Patagonia steppe (150–200 mm $year^{-1}$) (Godagnone and Bran, 2009) (**Figure 3A**). **Figure 4** shows the temporal variation of wind and total precipitation for VLA and IJ during the studied period (2011–2016). Whilst winds are stronger in IJ (∼3.5–7 m s^{-1}) than VLA (2–4 m s^{-1}), total precipitation is considerably higher in VLA (0.6–63 mm) than IJ (0–18 mm). Consequently, remobilisation is stronger in distal areas due to strong winds, low precipitation, low soil moisture, low vegetation cover and the abundance of fine ash. However, distal areas were strongly affected by ash remobilisation only until April 2014, when a strong precipitation occurred (**Figure 4B**), followed by a sharp reduction in the frequency of remobilisation events (Forte et al., 2018). This reduction is likely to have been caused by large-scale erosion of the primary deposit by surface water flow, although compaction of the primary deposit by particle re-arrangement may also have played a role.

We therefore focus on the deposits and physical characterisation of remobilised ash in the distal areas, particularly from PC to IJ. This region is characterised by three geomorphological units (Bran et al., 2009): (i) *Basaltic Plateau*, composed of Tertiary and Quaternary basalts, it is strongly exposed to wind and has a low vegetation cover (30–40%); (ii) *Mountains and Hills*, composed of Triassic and Jurassic volcanic and plutonic rocks, is covered by grass-dwarf shrubs and wetland vegetation; and (iii) *Depressions and Lowlands*, constituting typically low vegetated (10–30%) wide plains with some erodible bedforms.

There are two main types of remobilised-ash deposits: (i) deposits associated with non-erodible roughness elements, primordially vegetation and rocks, and (ii) deposits associated with pre-existing mounds. The dominant surface wind direction in the studied area is W-to-E, meaning both vegetation and sediment deposits have prevailing windward and leeward sides.

Deposits Associated With Roughness Elements (i.e., Vegetation and Rocks)

Ash accumulations in plants are the most commonly observed remobilisation deposit, with accumulation effectiveness depending on the species, quality, age and density of vegetation

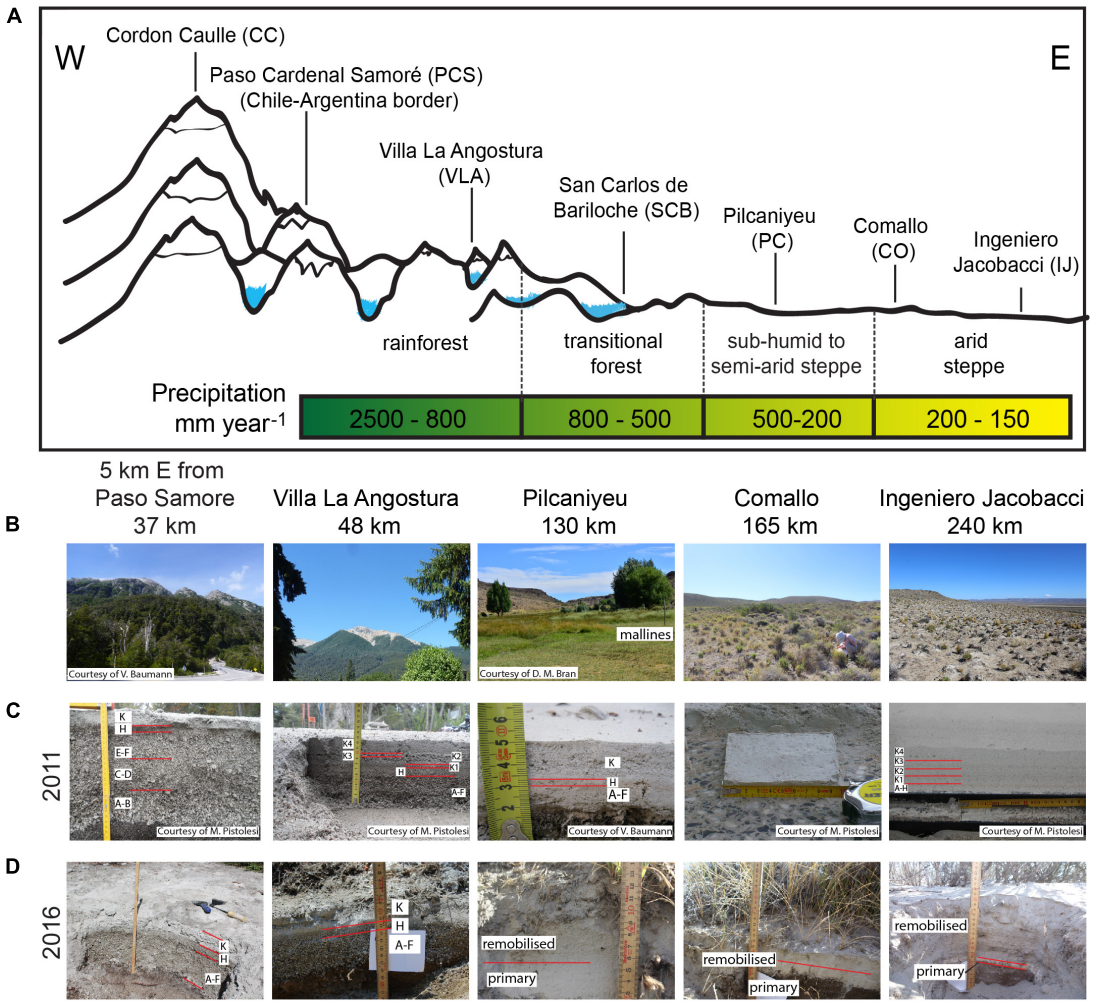

FIGURE 3 | (A) Schematised W-E transect showing the climatic gradient associated with precipitations and vegetation typology from the Andes range to the Patagonian steppe. Profile is indicative and not to scale. **(B)** Selected localities from proximal and distal areas showing the vegetation evolution along the transect (distances to the CC vent are indicated). **(C,D)** Primary tephra-fallout deposit at each location in 2011 and 2016, respectively.

cover (Kok et al., 2012). In the studied area, two main species of plants are identified (Edwards et al., 2017): grassy or herbaceous steppe (e.g., *Poa ligularis*, *Pappostipa speciosa*) of 0.2–0.5 m height (**Figure 5A**) and shrub steppe (e.g., *Prosopis denudans)* of 1–2 m height (**Figure 5B**). Additionally, large interpatch areas (bare soil between plants), showing strong erosion surfaces, are common (**Figure 5C**). Both herbaceous or shrub plants can either be isolated and surrounded by bare soil due to high erosion (**Figure 5A**) or in patches of specimens covering surfaces up to 15 m^2 (**Figure 5B**). Deposition occurs on both windward and leeward sides, as well as inside the plant, where ash is incorporated by the soil. Generally, deposits are thicker and larger on the leeward side compared to the windward. Thickness can vary from 2–5 cm in windward areas (**Figure 5D**) to up to 30 cm in leeward areas (**Figure 5E**). **Figures 5D–F** show the main sedimentary structures on both windward and leeward sides as well as within the interpatch area. The most removable material is eroded from the uncovered interpatch areas and is subsequently deposited inside and around the plant. Laminar stratification can be present (**Figure 5F**) and dry cracks are very common (**Figure 5C**). Windward and leeward deposits are characterised by small-scale cross stratification which is more evident in the leeward side (**Figure 5E**).

Although less frequent, remobilised ash also accumulates around other roughness elements such as rocks (**Figure 5G**). Whilst vegetation is an open structure, rocks act as solid windbreaks, meaning that fine ash accumulates in the cavities surrounding the rock. These deposits are small pockets of very fine ash with no micro-structures and were mostly observed on the leeward side of rocks, being uncommon on the windward side.

Deposits Associated With Pre-existing Mounds

Though patchy accumulations of remobilised ash can occur in the basaltic plateau and mountainous areas, the most abundant deposits are associated with the Depression and

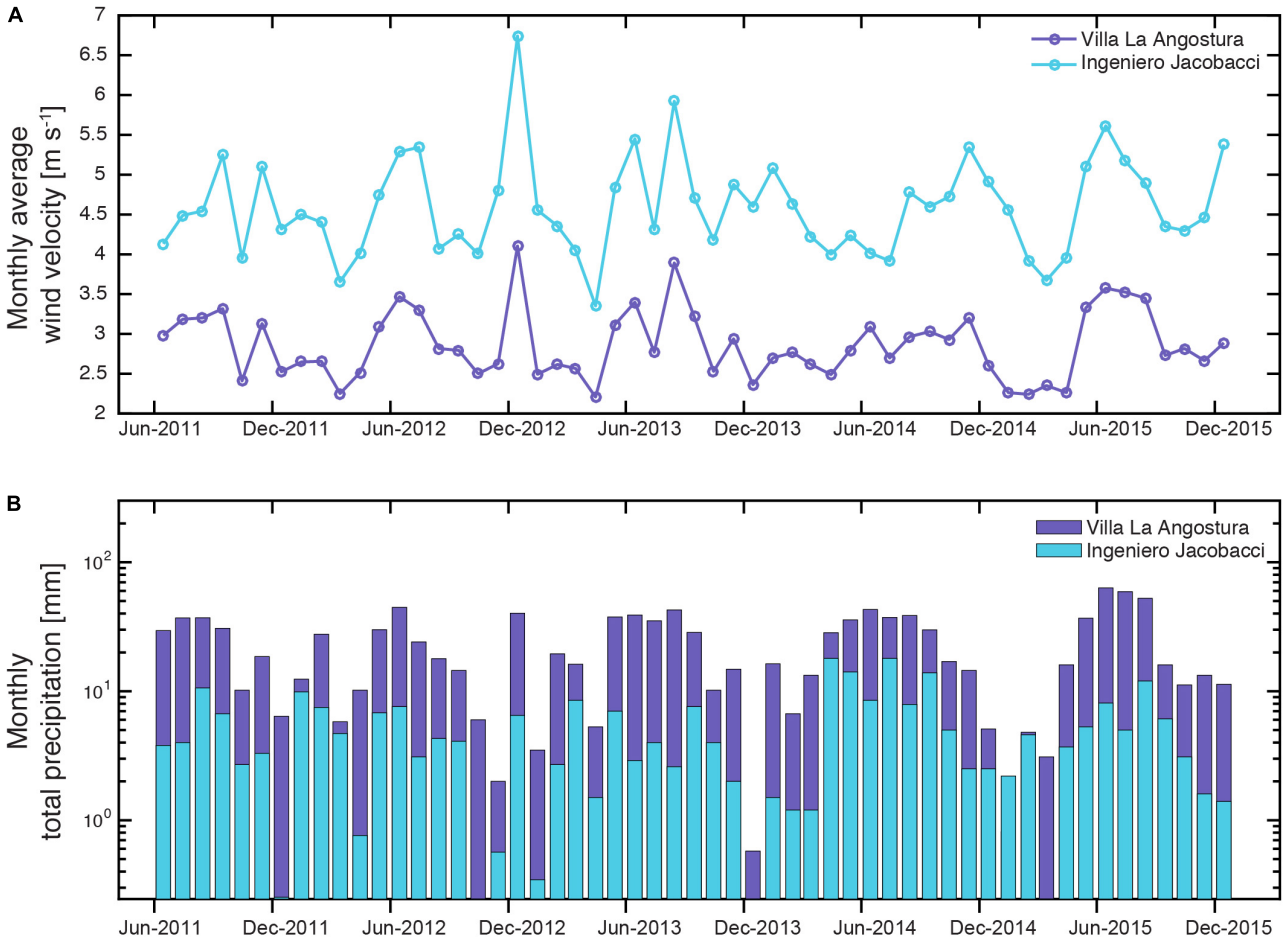

FIGURE 4 | (A) Monthly averaged wind velocity and **(B)** monthly total precipitation for two localities, Villa la Angostura and Ingeniero Jacobacci. Prevailing wind direction is west to east. Meteorological data from the ECMWF (European Centre for Medium-range Weather Forecasts) ERA-Interim reanalysis dataset.

Lowlands geomorphological unit. These areas consist of large dunes (10–20 m^2 horizontal area), mounds and other erodible bedforms constituted by the bedrock covered by volcaniclastic sediments and sand.

Field observations from 2016 showed that upper layers of pre-existing mounds were composed of a mixture of sand, old volcanic sediments and the 2011-CC fresh ash. **Figure 5H** shows a large mound of erodible material composed of such a mixture. **Figure 5I** shows a typical leeward side of a sandy mound composed of several layers of sand and ash, including a distinguishable massive layer (≈2 cm) composed entirely of 2011-CC ash. This layer could correspond to a stratigraphic record of the primary tephra deposit on the top of the mound in 2011 although it is difficult to determine if syn- or post-depositional aeolian processes also took place. On top is a 20 cm loose mixture composed of ash and sand with clear cross-stratification structures. Profiles of the leeward side of two mounds are presented in **Figures 5J,K**. Here, ash is preserved as either small fine-ash pockets or lenses of length <10 cm embedded in a massive sandy matrix (**Figure 5J**) or inhomogeneous, coarse-ash cross-stratified layers (<20 cm thickness) intercalated with fine-ash lenses (**Figure 5K**). **Figure 5L** shows accumulations of very fine and highly cohesive particles covering the surface of slopes. These accumulations, very similar to the fine-ash lenses in **Figures 5J,K**, often display red oxidation lines on the uppermost surfaces.

Physical Characterisation of Particles

Grainsize Analysis

Weight-averaged grainsize distributions (GSDs) of both ground and airborne samples are shown in **Figure 6**. All remobilised samples present unimodal platykurtic and positive- to very positive-skewed distributions. For comparison, distributions for the proximal and the distal primary Unit III are also displayed. The proximal distribution is bimodal with two modes (1.1 mm and 40 μm), whilst the distal is unimodal with a mode at 45 μm. The fraction material < 125 μm is considerably higher in distal (99% in volume) than in proximal (∼29% in volume) areas.

We distinguish between GSDs for deposits associated with vegetation and rocks (**Figure 6A**) and mounds (**Figure 6B**). **Figure 5A** shows that the leeward sides of plants are coarser than

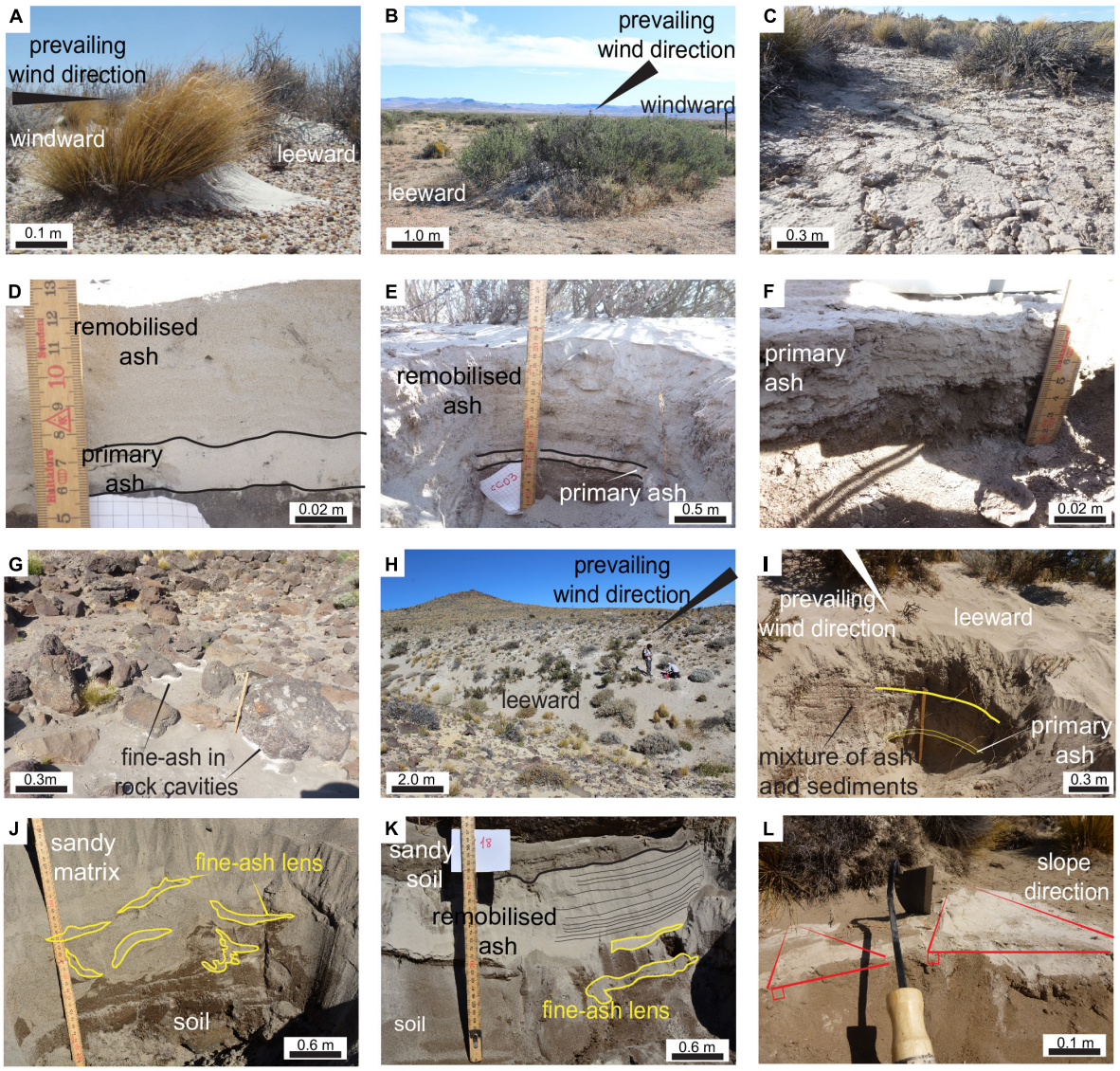

FIGURE 5 | Remobilisation deposits: **(A)** Deposit on the leeward side of an herbaceous steppe plant (*poa ligularis*) (Photo: Juan Gaitan). **(B)** Leeward side deposit on bank of plants (*prosopis denudans*). **(C)** Interpatch surface between plants. **(D)** Primary and remobilised deposit on the windward side of a group of plants. **(E)** Primary and remobilised deposit on the leeward side of a group of plants. **(F)** Planar stratificated deposits within the interpatch surface. **(G)** Accumulations of very fine ash in cavities between rocks. **(H)** Overview of the leeward side of a large bedform. **(I)** Remobilised deposits on the leeward side of a mound. **(J)** Fine-ash lenses embed in a sand-ashy matrix. **(K)** Cross stratified layer of remobilised ash intercalated with fine-ash lenses. **(L)** Accumulation of very fine-ash on the slopes of a dune.

windward sides, with an increased mode from 45 to 90 μm. The finest material is found in interpatch areas, with a mode of about 30 μm. The GSD of rock cavity ash is very similar to the primary distal GSD, with a mode about 35 μm. For the deposits associated with mounds (**Figure 6B**), two contrasting granulometries are present; fine-ash lenses with typical modes of 30 μm are intercalated with coarse-ash mound layers with modes of 95 μm. The grainsize of airborne samples (**Figure 6C**) shows very similar and narrow distributions regardless of the distance from the vent. Though these samples have been collected in proximal (S2) and distal (S6) areas (**Figure 2B**), their granulometry is very similar, with a constant mode of about 65 μm for all the distributions.

All remobilised samples are very well- to well-sorted (α_ϕ = 0.79–1.63) (**Figures 7A,B**) while the primary Unit III is poorly sorted in proximal areas (1.20 < α_ϕ < 3.54) and well sorted distally (α_ϕ = 1.5). Sorting is calculated as the Inman graphic standard deviation in phi units according to, α_ϕ = (P84–P16)/2 where P16 and P84 correspond to 16th and 84th percentiles, respectively (Inman, 1952). Additionally, while Md_ϕ of Unit III varies from −2 to 5ϕ (4000–32 μm) proximally, it is 5ϕ (30 μm) in distal areas (Md_ϕ is the median diameter in ϕ scale where $\phi = -\log_2 D/D_0$, and D_0 = 1 mm). **Figure 7A** also shows that rock accumulations, interpatch areas and fine-ash lenses (associated with mounds) are granulometrically very similar to

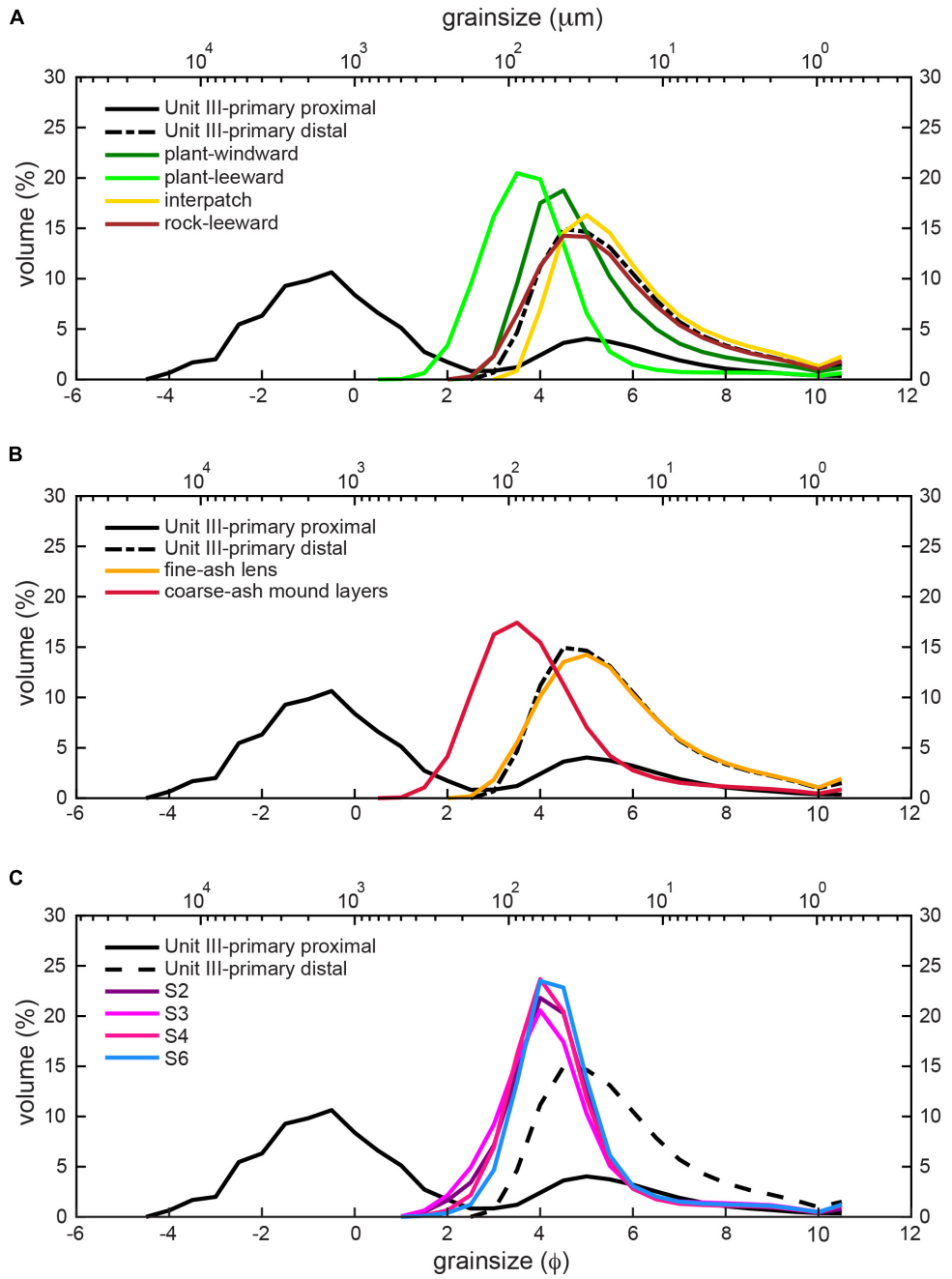

FIGURE 6 | Weight-averaged grainsize distributions of primary tephra fallout (i.e., Unit III – proximal and Unit III – distal corresponding with ∼100 and ∼300 km from the vent, respectively) and remobilised ash deposits associated with: **(A)** roughness elements (i.e., ground samples, Dataset 1); **(B)** pre-existing mounds (i.e., ground samples, Dataset 1); **(C)** airborne samples for the four selected sites (i.e., Dataset 2). The *x*-axes are displayed in phi-scale (bottom) and microns (top), $\phi = -\log_2 D/D_0$, where $D_0 = 1$ mm.

the primary distal Unit III. Plant-associated deposits, particularly in the leeward sides, show better sorting (α_ϕ = 0.8) than the primary distal Unit III. The airborne samples are characterised by very well-sorted samples with median sizes of 40–92 μm (Md_ϕ = 3.4–4ϕ and α_ϕ = 0.8–1.5; **Figure 7B**). In particular, samples collected at higher positions (1.50 m) are better sorted than those collected lower (0.15 m), whilst, as expected, the grainsize decreases with height with the material collected at 0.15 m slightly coarser than that at 1.50 m (**Figure 7C**). Finally, the grainsize slightly increases over time for all collectors, as demonstrated for collector S3 in **Figure 7D**. Detailed grainsize data are presented in **Table 3** and **Supplementary Table S1**.

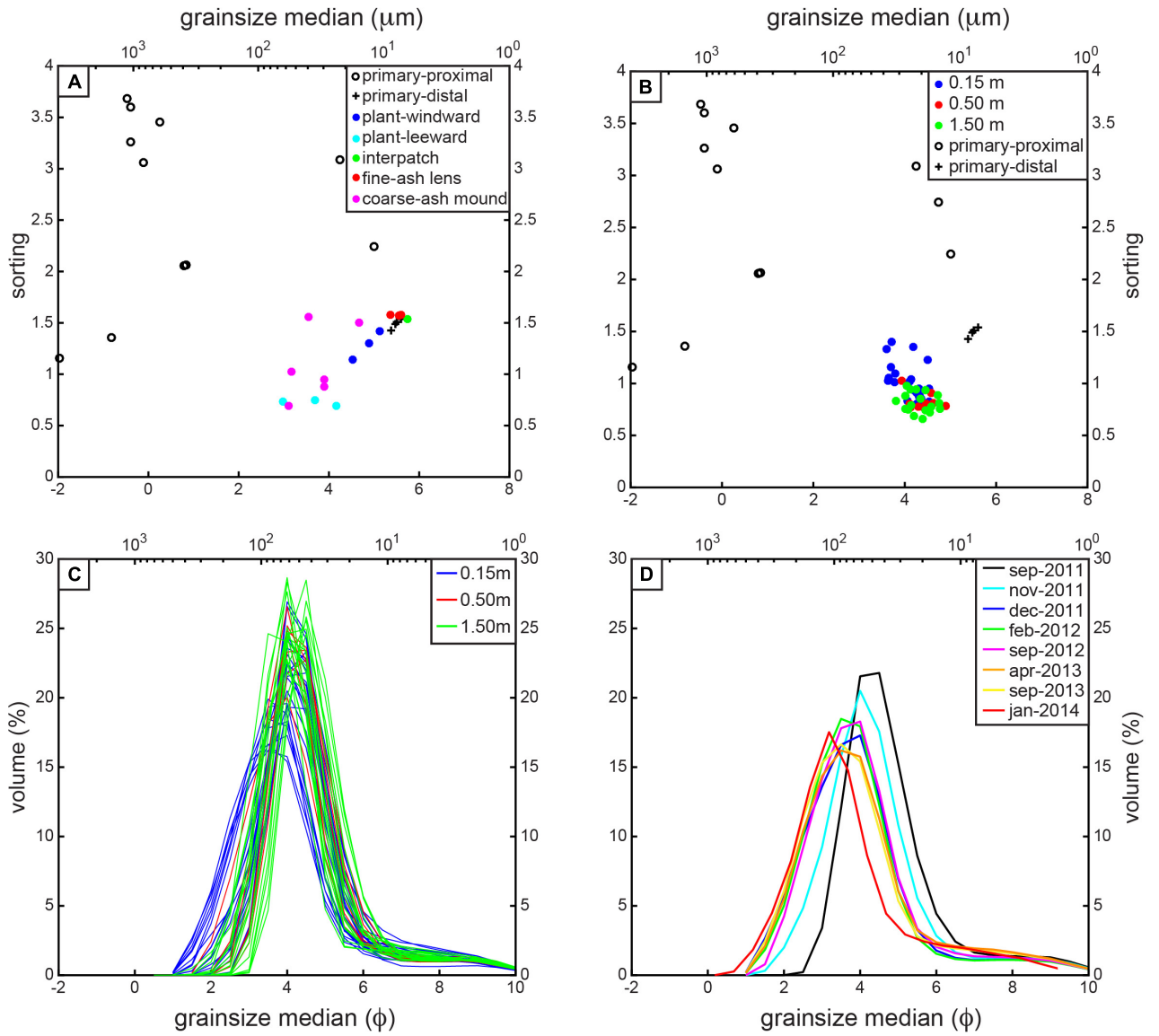

FIGURE 7 | Grainsize comparison between primary (i.e., Unit III) and remobilised ash: median grainsize versus sorting for the **(A)** ground samples and **(B)** airborne samples differentiated by type of deposit and collector height; **(C)** GSDs of the airborne samples for different collector heights; **(D)** evolution of grainsize as a function of time for airborne samples at the site S3. All *x*-axes are displayed in phi-scale (bottom) and microns (top), $\phi = -\log_2 D/D_0$, where $D_0 = 1$ mm. Sorting, calculated as the Inman graphic standard deviation in phi units, $\alpha_\phi = (P84 - P16)/2$ where P16 and P84 correspond to 16th and 84th percentiles, respectively (Inman, 1952).

Shape Analysis

Backscattered-electron images of both primary distal Unit III and remobilised material, classified by phi classes, are presented in **Figure 8**. Primary ash <125 μm (class 1 and 2) is composed of highly vesicular and irregular pumices with planar external surfaces and sharp edges. In contrast, remobilised ash of the same size shows sub-angular to sub-rounded shapes with smoother edges and surfaces. Coarse ash (class 3) from both primary and remobilised deposits shows similar shapes, being mainly composed of angular and irregular shards with conchoidal fractures. Non-volcanic materials, such as pellets, are present in all remobilised classes (**Figure 8**).

In classes 1 and 2, remobilised particles have slightly higher median values of solidity than the primary particles (**Figure 9A**), with class 2 (63–125 μm) showing the largest difference (0.77–0.83). Class 3 shows no change in solidity, indicating that for large particles solidity is less affected by remobilisation processes. Convexity values show different trends in different size classes (**Figure 9B**). For class 1, remobilised ash has a smaller convexity and higher variability than the primary ash, whilst the opposite is true for class 2. Again, remobilised and primary particles in class 3 show no difference in convexity. Primary ash in classes 1 and 3 have a slightly larger circularity than remobilised ash (**Figure 9C**), whilst remobilised particles in class 2 are much more circular than

TABLE 3 | Averaged volume percentage (%) per grainsize class for primary tephra-fallout deposit and remobilised samples.

Type of deposit	0.4–20 μm	20–63 μm	63–125 μm	125–500 μm	>500 μm	Total < 63 μm	Total 63–500 μm
Primary deposit – Unit III							
Primary proximal	13	11	4	6	66	24	76
Primary distal	41	43	15	1	–	84	17
Remobilised-associated material							
Plant – windward	27	44	27	2	–	71	29
Plant – leeward	7	23	40	30	0.03	30	70
Interpatch	47	45	8	0	–	92	7
Rock – leeward	39	41	17	3	–	80	21
Fine – ash lens	42	41	15	2	–	83	17
Coarse – ash dune layers	13	22	33	32	0.07	35	65
Airborne – 0.15 m	13	34	37	16	–	47	53
Airborne – 0.50 m	14	42	37	7	–	56	44
Airborne – 1.50 m	14	41	38	7	–	55	45

their primary equivalents, with a circularity of 0.83 as opposed to 0.70. Detailed shape data are presented in **Supplementary Table S2** and **Supplementary Figure S2**.

DISCUSSION

Particle Size and Shape Analysis: Implications for Transport Mechanisms

Modelling of dust and sand erosion of the last few decades (Pye, 1987; Shao and Lu, 2000; Shao, 2008; Kok et al., 2012; Újvári et al., 2016) is fundamental to our understanding of transport mechanisms associated with ash remobilisation. Although different transport mechanisms are typically associated with theoretical grainsizes [long-term suspension, <20 μm; short-term suspension 20–70 μm; saltation, 70–500 μm; creep,>500 μm (Pye, 1987)], the role of wind friction velocity and soil properties means the grainsize-transport mechanism relationship is complex with smooth and gradual transitions (Shao, 2008; Újvári et al., 2016). Consequently, in this section, we cautiously combine these theoretical thresholds with a detailed comparative analysis of particle size and shape between the primary tephra-fallout and the remobilised deposits to determine the dominant transport mechanisms. In the next section, we combine these results with field observations to interpret the probable formation processes of the analysed deposits in the Patagonian steppe.

Our grainsize analysis shows that wind can remobilise particles with a very specific size range (<0.4 to 500 μm), with values of distribution median of 25–135 μm and modes of 30–95 μm (**Figures 6**, **7** and **Supplementary Table S1**). For the airborne samples, measured grainsize slightly decreases with height, with the 97.5th percentile rapidly decreasing from 250 μm at 0.15 m to 150 μm at 0.50 m, and more gradually to 144 μm at 1.50 m (**Supplementary Table S1**). Grainsize analysis alone does not conclusively indicate a predominant transport mechanism; the material coarser than 63 μm (most likely associated with saltation) is 53% in the collector at 0.15 m and 44 and 45% in the collectors at 0.50 and 1.50 m, respectively, suggesting that suspension becomes more significant with height. Approximately 42% of all airborne material is in the range 20–63 μm, compared to 14% in the range of 0.4–20 μm, suggesting short-term suspension dominates over long-term suspension. Finally, the fact that grainsize has generally increased from 2011 to 2014 (**Figure 7D**) suggests that fine particles have been remobilised from the studied area, most likely toward the East due to the prevailing winds. Since the size that minimises the threshold friction velocity corresponds to the class 2 (63–125 μm), we expect a significant depletion of these particles in the primary deposit. The complex relation between saltation and suspension induced by saltators might provoke also the depletion of the finer fraction (<63 μm) with time. As a consequence, coarser particles remain in the surface for longer periods because they can only be removed during periods of strong winds. Since all the particles of the Unit III are potentially remobilisable by wind, we might expect a complete erosion of this unit with time, with the exception of the locations were this deposit is well preserved (protected by vegetation or wetlands).

Grainsize comparison (**Figures 7A,B**, **Table 3** and **Supplementary Table S1**) suggests that ground samples from interpatch areas between non-erodible roughness elements are slightly enriched in fine particles and depleted in coarser (>63 μm), from 7% of interpatch deposits compared to 17% in primary equivalents. Additionally, windward and leeward deposits around plants have contrasting granulometry. Windward sides are enriched in fine material, with 71% of material <63 μm, and 44% in the range 20–63 μm, whilst 70% of material on the leeward side is >63 μm. This suggests that windward material has mainly deposited from suspended particles from the interpatch (particularly short-term suspension), whereas saltators have crossed the plants to the leeward side. Deposits associated with mounds contain two contrasting structures, fine-ash lenses (83% of material < 63 μm) and coarse-ash dune layers (65% in range 63–500 μm). These most likely originate from an interaction amongst wind flow, topography and particle transport, although further

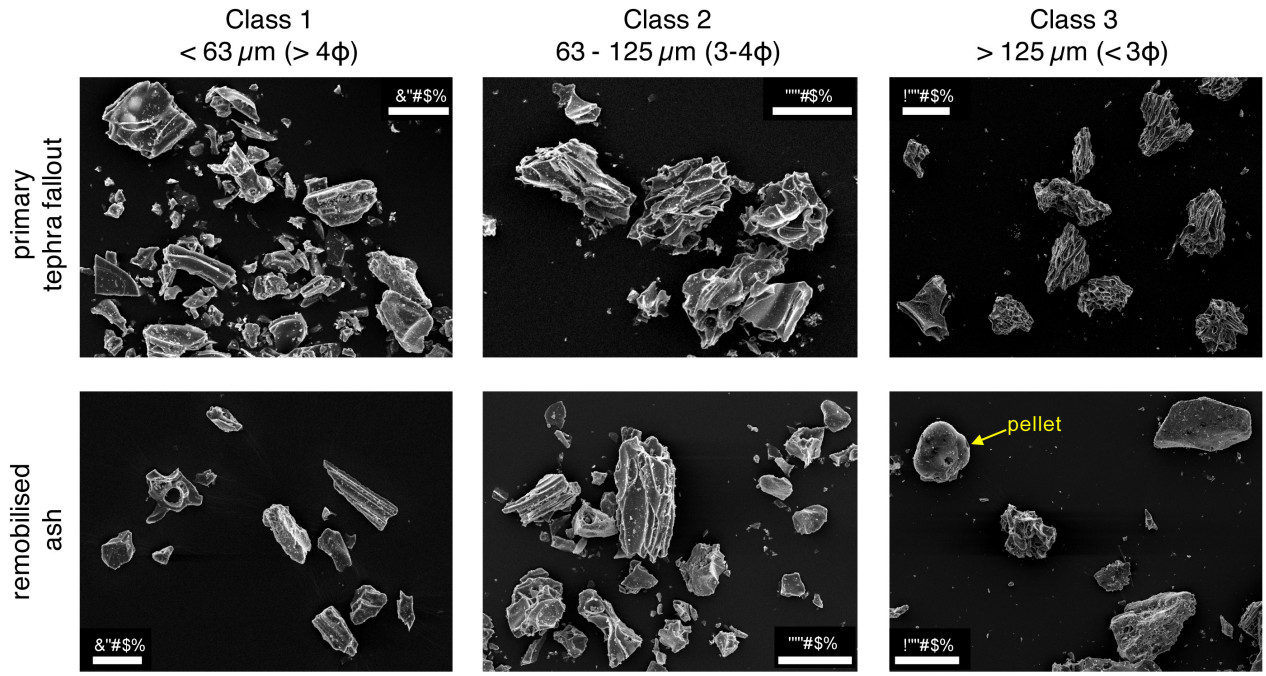

FIGURE 8 | Backscattered SEM images of primary tephra-fallout and remobilised ash particles classified by phi classes.

interpretation combining field observations is presented in Section 'Interpretation of Ash-Remobilised Deposits in the Patagonian Steppe'.

Additionally, we find that about 15–40% by volume of remobilised material has a grainsize of 63–125 μm. By comparison, this size range only accounts for 4 and 16% of the primary proximal and distal deposits, respectively, suggesting that this fraction has been significantly remobilised. In fact, this size corresponds to that which minimises the threshold friction velocity (**Figure 10A**) (Shao, 2008; Kok et al., 2012). Interestingly, our detailed shape analysis has also shown that remobilised class 2 particles (63–125 μm) have the most significant increase in all shape descriptors compared to the primary particles (**Figure 10**). In contrast, remobilised ash in class 1 (<63 μm) have slightly larger solidities and lower circularities than the equivalent primary ash, whilst class 3 (>125 μm) shows little morphological variation suggesting almost negligible transport effect. Since particles of class 2 are of the size that minimises the threshold friction velocity (**Figure 10A**), they are most likely transported by saltation and become abraded and, therefore, have higher convexity, solidity and circularity than primary ash (**Figure 10B**, **Supplementary Table S2** and **Supplementary Figure S2**). Remobilised class 1 particles, in part ejected by saltator impacts, might be transported in suspension and experience less abrasion than the saltated fraction, showing larger solidity but smaller circularity and convexity (rougher surfaces) than the equivalent primary ash.

We also observe ash morphology variations between different sample locations for class 2 particles (**Figure 10B**). Airborne ash and that associated with plant deposits show higher values of both solidity and convexity compared to primary ash, indicating that this material has possibly travelled long distances undergoing major abrasion with resulting higher roundness values. Abrasion might also create very fine ash (dust), slightly increasing the amount of material readily available for suspension. In fact, this confirms that suspension might control transport mechanisms of airborne material. The generation of new PM10 material due to abrasion, combined with the likely breakage of particle clusters formed during primary fallout, means wind remobilised ash events can be more impacting on public health than the associated primary fallout (e.g., Baxter et al., 1999). In contrast, samples associated with mounds, i.e., coarse-ash dune layers and fine-ash lenses, have similar solidity and convexity values with respect to the primary ash (**Figure 10B**). In fact, coarse-ash dune layer samples have slightly lower solidity than primary ash, suggesting that this material is only transported locally and possibly contains fragments of broken particles with more angular shapes. Grainsize and shape of fine-ash lenses are very similar to those of primary ash but slightly enriched in fine material. This could be associated with local granular segregation and consequently, little wind transport that did not affect particle shape. Another possible interpretation is that these lenses represent remnant portions of a partially eroded primary deposit.

Interpretation of Ash-Remobilised Deposits in the Patagonian Steppe

wind-remobilisation of volcanic ash is a special case of erosion, typically involving a mixture of old volcaniclastic sediments

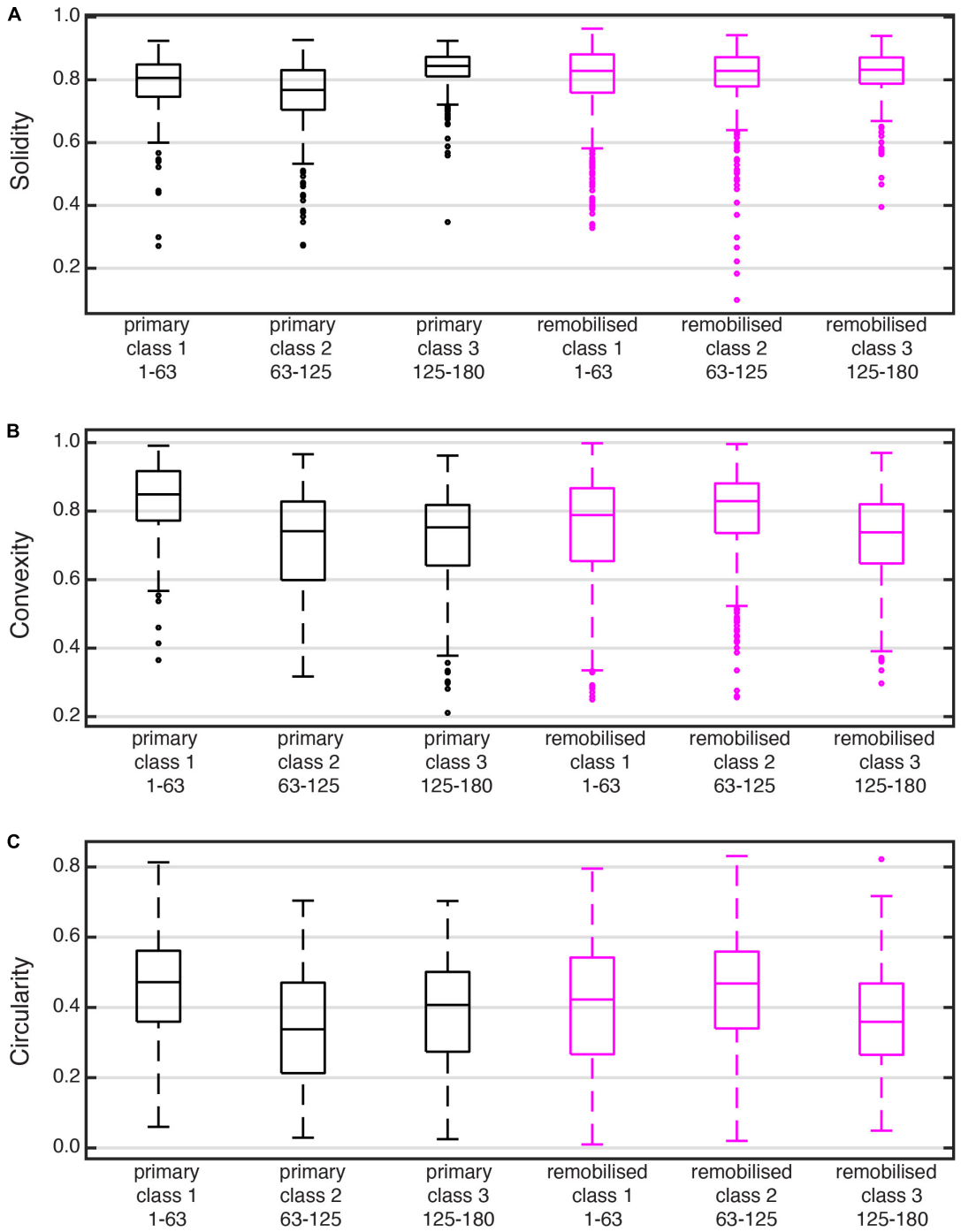

FIGURE 9 | Box and whisker plots showing comparison of **(A)** solidity, **(B)** convexity, and **(C)** circularity for primary and remobilised ash. The three parameters are dimensionless and scaled from 0 to 1, being 1 the perfect circle. Lower and upper edges of each box indicate the 25 and 75% percentiles, respectively, with the middle line corresponding to the median. Box width represents the variability of values within the same sample. The whiskers extend to the most extreme values and the points correspond to outliers.

and fresh deposits, resulting in complex depositional structures. Associated transport mechanisms can be derived based on a combination of grainsize features and deposit morphologies. In particular, we investigate deposits associated with non-erodible roughness elements (**Figures 11A–C**, vegetation and rocks) and with pre-existing mounds (**Figures 11D–F**).

Any non-erodible roughness elements, such as rocks, plants or artificial structures, act as windbreaks, absorbing wind

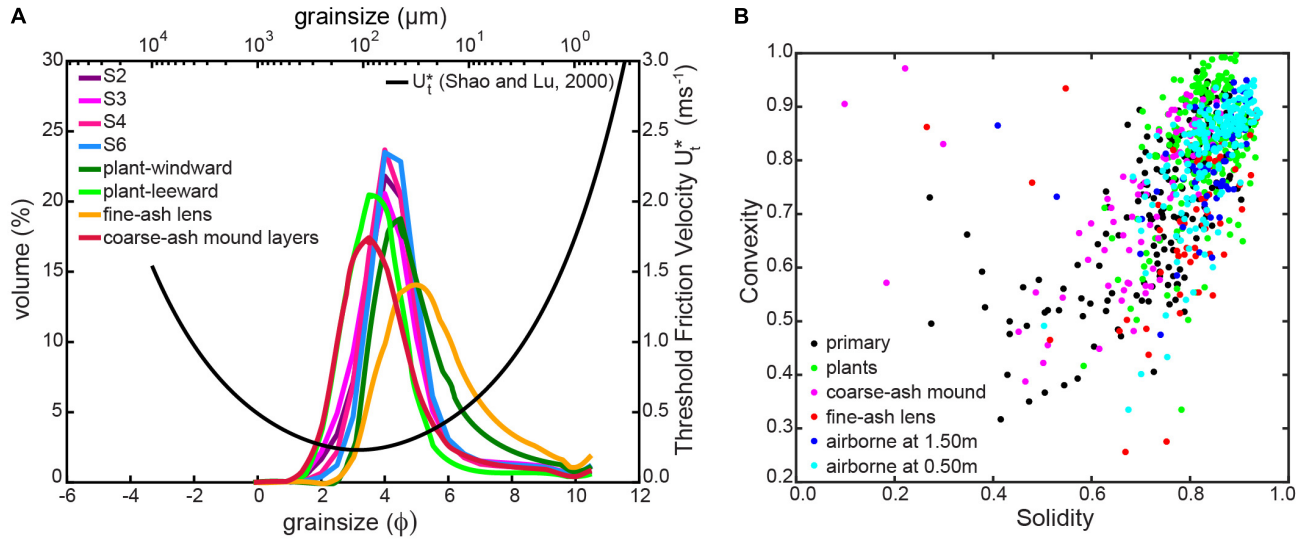

FIGURE 10 | (A) Grainsize distributions of ground (plants, ash lenses and mound layers) and airborne (sites S2, S3, S4, S6) samples and the theoretical threshold friction velocity U^*_t (Shao and Lu, 2000). **(B)** Solidity and convexity values for the different types of remobilised samples for size class 2 (63–125 μm), which is the class with the largest variation in both parameters.

momentum and reducing wind friction velocities (Shao, 2008; Kok et al., 2012; UNEP et al., 2016). Plants, for example, inhibit erosion, enhance deposition and preserve primary ash deposits due to their high capacity of soil assimilation. Interpatches are typically detachment areas (Kok et al., 2012) representing the primary deposit remnants where sand-sized (>63 μm) particles initiate motion by saltation, resulting in laminar-stratified layers typically composed of finer and very well sorted material (mode, 30 μm) (**Figure 10A**). Saltator impacts might also induce the short-term suspension of smaller particles (20–70 μm). Interaction between the wind and the roughness elements governs the local deposit characteristics. Wind streamlines diverge around obstacles and become compressed (Shao, 2008), producing faster wind velocities around the plants that can lift even small grains. Particles settle when they reach a stagnation point (i.e., negligible friction velocity), generally at the front and back of obstacles (**Figures 9B,C**), generating fine-ash and well-sorted deposits on the windward side of the plant. A larger stagnation exists on the leeward side, upwind of where the streamlines converge, generating larger, thicker, coarser and better sorted deposits (mode, 90 μm) compared to the windward sides (mode, 45 μm). Cross-stratified structures record the intermittent and long-lasting sediment transport and deposition in these deposits.

Field observations suggest that laminar-flow regimes are favoured by open structures, i.e., vegetation (**Figure 11B**), while turbulent-flow regimes are associated with solid or closed elements, i.e., rocks (**Figure 11C**). In the case of open structures, associated with vegetation, particles get trapped and assimilated within the roots to different degrees depending on the species, density cover, canopy height, age, structure connectivity or root distribution (Shao, 2008). Larger deposits are associated with young plants growing in groups rather than individual specimens or old plants due to their parallel and highly connected structure with a greater capacity for ash storage. Closed elements such as rocks generate turbulent-flow regimes with turbulent eddies shedding from the rock surface (Shao, 2008). These flow structures on the leeward side might produce granular segregation (**Figure 11C**), with larger particles saltating in the flow direction whilst very fine particles (mode, 35 μm) become trapped in eddies and fail to escape the stagnation zone, filling the leeward cavities of the rock. Granulometry of these small deposits is almost identical to the primary distal deposits (**Figure 6A**), suggesting that these particles are transported across very short distances from the primary source.

Ash-remobilisation deposits associated with mounds require more careful interpretation (**Figures 11D–F**). Cross lamination and stratification structures might be related to the saltation-creep processes inherent to dunes and ripples (Bagnold, 1941; Mcphie et al., 1993; Kok et al., 2012) where saltating particles generate small depressions that, during low-flow regimes, can capture smaller particles (**Figure 11E**). Wind streamlines become compressed as they climb the windward slope, with the wind velocity reaching its maximum value at the crest (Shao, 2008). Consequently, both fine and coarse material can be carried over the dune by the wind. Flow separation at the crest forms a shadow zone on the leeward side where deposition occurs (**Figure 11F**). This region is typically described as a clockwise recirculation bubble where eddies are common (Shao, 2008; Kok et al., 2012). These eddies and the complex flow circulation are responsible for sporadically increased velocities which might provoke granular segregation. We interpret that fine particles, predominantly fresh ash, might roll down until they reach a stagnation point, probably induced by intermittent high-flow and no-wind regimes. In fact, rolling particles are more protected from saltator impacts in the

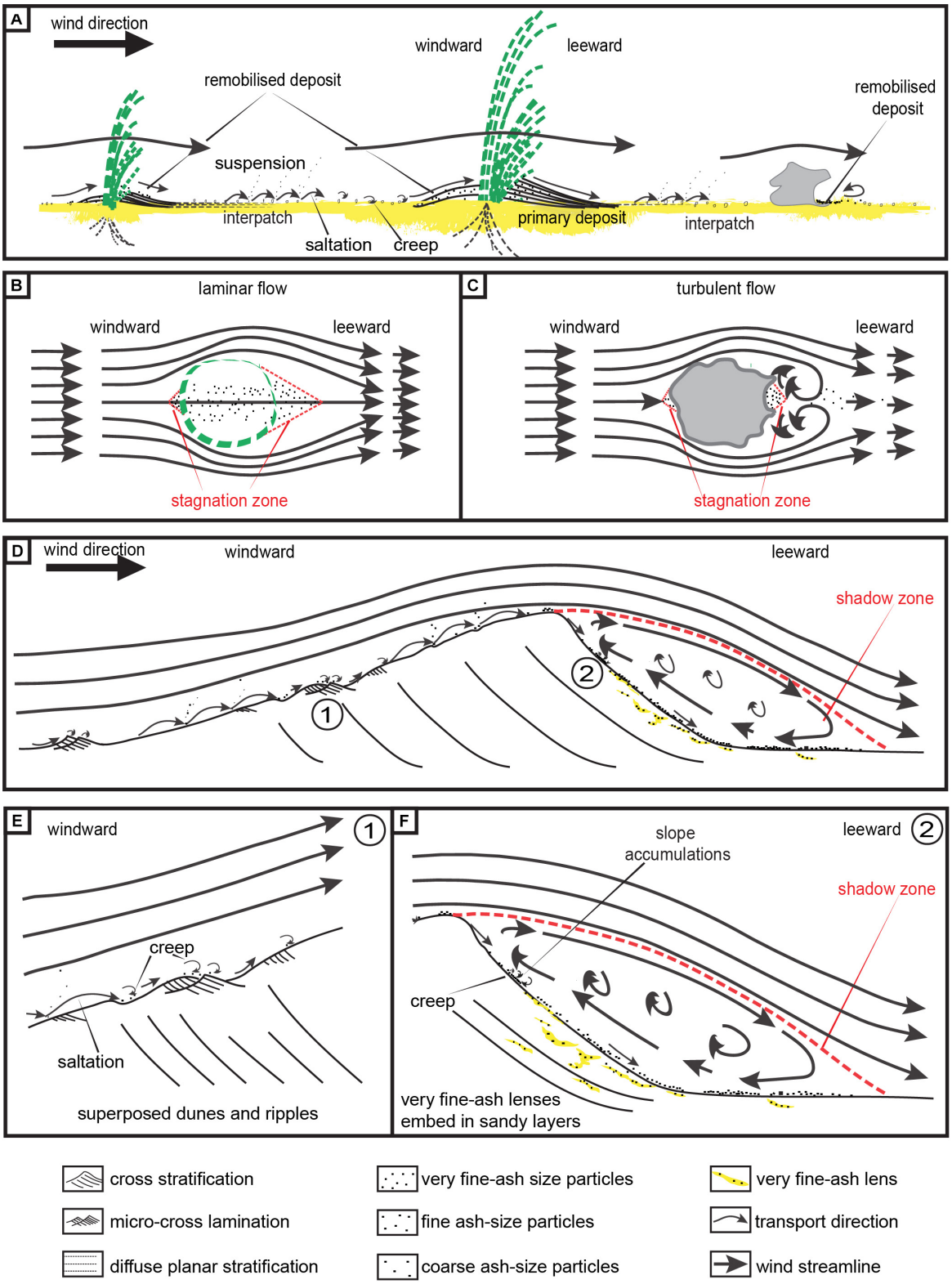

FIGURE 11 | Cartoons showing transport and deposition mechanisms for remobilised ash: **(A)** deposits associated with roughness elements (e.g., vegetation and rocks); plan view of processes associated with **(B)** laminar and **(C)** turbulent flow regimes; **(D)** ash remobilisation processes associated with pre-existing mounds; **(E)** detailed view of ripple formation (label 1 in **D**); **(F)** detailed view of shadow zone processes (label 2 in **D**). Bold arrows indicate wind streamlines. Cartoons not to scale.

leeward side compared to the windward region (Shao, 2008). The highly cohesive forces of smaller particles (i.e., mode 30 μm) might favour their assembling and formation of small lenses (i.e., length < 10 cm). Coarser material, composed of sand and coarse ash, might follow the dune deposition processes. As a result, small-scale structures of very fine-ash (i.e., very good sorting; mode of 30 μm) superposed with sandy cross-stratified layers (i.e., good sorting; mode of 95 μm) are present in these deposits. Alternatively, these lenses could simply represent the remnant of a partially eroded primary deposit, where coarse and easily removable material has been transported following dune processes, while fine particles, given their highly cohesive forces, have little or no transport. Both could be plausible explanations of these deposits although other complexities, such as the role of water-driven erosion, have not been considered here.

Our results demonstrate that although particle (size and shape) and deposit features (morphology and structures) alone are insufficient to interpret transport mechanisms, the combined approach of both along with theoretical sediment transport considerations, provides important insights into ash remobilisation. However, the fact that explosive volcanic eruptions generate a large volume of loose fine material that significantly modifies the surface properties on a short timescale means that the erosion of fresh volcanic material significantly differs from that typically considered in dust and sand models. As such, the correlation of the primary volcanic source with the associated remobilised deposits is also fundamental to understand the life cycle of volcanic ash.

CONCLUSION

Our comprehensive study of remobilisation deposits and of the physical characteristics of associated particles provides new insights into an important process of the volcanic ash life cycle that represents a threat to communities even many years after an eruptive event. We have developed a classification for volcanic remobilisation phenomena consistent with the WMO classification of lithometeors (WMO, 1975). In particular, we suggest that the widely used term 'ash resuspension' should only be used to describe transport by suspension, while aeolian ash remobilisation and ash wind-remobilisation can be used to indicate the overall process (including deposition).

Additionally, we have shown how transport mechanisms can be inferred based on a combined study of deposit morphology with particle grainsize and shape. For the example of the 2011-CC tephra-fallout deposit, we have inferred that the majority of remobilisation occurs through saltation, although suspension, mostly triggered by saltator impacts, plays also a role.

Further studies involving measurements of meteorological conditions and surface properties are essential to advance in our understanding of ash wind-remobilisation. The complexity of this stage of the life cycle of volcanic ash requires multi-disciplinary studies between volcanologists and soil erosion, climate and atmospheric scientists harmonising nomenclature, definitions and research approaches.

DATA AVAILABILITY STATEMENT

All datasets generated for this study are included in the article/**Supplementary Material**. Additional raw data are available upon request.

AUTHOR CONTRIBUTIONS

LD, PF, and DB conducted field work and ground sampling under CB supervision. DB and JP collected airborne material. LD performed grainsize and shape analysis, data processing and the elaboration of the manuscript. All authors were involved in data interpretation as well as the refinement of this article.

FUNDING

This work was supported by the Swiss National Science Foundation (#200021_163152). Sampling of airborne material is part of the National Soil Research Program of INTA.

ACKNOWLEDGMENTS

We thank Donald Mauricio Bran and Jazmin Miguel for their support in the field and Valerie Baumann and Manuela Elissondo for their insightful and constructive discussions.

SUPPLEMENTARY MATERIAL

The Supplementary Material for this article can be found online at: https://www.frontiersin.org/articles/10.3389/feart.2019.00343/full#supplementary-material

REFERENCES

Arnalds, O., Thorarinsdottir, E. F., Thorsson, J., Waldhauserova, P. D., and Agustsdottir, A. M. (2013). An extreme wind erosion event of the fresh Eyjafjallajökull 2010 volcanic ash. *Sci. Rep.* 3:1257. doi: 10.1038/srep01257

Bagnato, E., Aiuppa, A., Bertagnini, A., Bonadonna, C., Cioni, R., Pistolesi, M., et al. (2013). Scavening of sulphur, halogens and trace metals by volcanic ash: the 2010 Eyjafjajökull eruption. *Geochim. Cosmochim. Acta* 103, 138–160. doi: 10.1016/j.gca.2012.10.048

Bagnold, R. A. (1941). *The Physics of Blown and Desert Dunes*, 1st editon Edn. New York, NY: Methuen.

Barsotti, S., Andronico, D., Neri, A., Del Carlo, P., Baxter, P. J., Aspinall, W. P., et al. (2010). Quantitative assessment of volcanic ash hazards for health and infrastructure at Mt. Etna (Italy) by numerical simulation. *J. Volcanol. Geotherm. Res.* 192, 85–96. doi: 10.1016/j.jvolgeores.2010.02.011

Baxter, P., Bonadonna, C., Dupree, R., Hards, V. L., Kohn, S. C., Murphy, M. D., et al. (1999). Cristobalite in Volcanic Ash of the Soufrière Hills Volcano,

Montserrat, British West Indies. *Science* 283, 1142–1145. doi: 10.1126/science.283.5405.1142

Baxter, P., and Horwell, C. (2015). "Impacts of eruptions on human health," in *The Encyclopedia of Volcanoes*, eds H. Sigurdsson, B. Houghton, S. McNutt, H. Rymer, and J. Stix (Amsterdam: Elsevier).

Bitschene, P. R. (1995). "Environmental impact and hazard assessment of the August 1991 eruption of Mt. Hudson (Patagonian Andes)," in *The August 1991 Eruption of the Hudson Volcano (Patagonian Andes): A Thousand Days After* eds P. R. Bitschene and J. Menida (Gottinge: Cuvillier Verlag), 2–15.

Bonadonna, C., Cioni, R., Pistolesi, M., Elissondo, M., and Baumann, V. (2015). Sedimentation of long-lasting wind-affected volcanic plumes: the example of the 2011 rhyolitic Cordón Caulle eruption. Chile. *Bull. Volcanol.* 77:13. doi: 10.1007/s00445-015-0900-8

Bran, D. E., Velasco, V., Lopez, D., Gaitan, J. J., and Quiroga, S. (2009). *Región Patagonia Sitio Piloto Jacobacci Estación Experimental Agropecuaria INTA Bariloche*. Bariloche: INTA EEA.

Butwin, M. K., von Löwis, S., Pfeffer, M. A., and Thorsteinsson, T. (2019). The effects of volcanic eruptions on the frequency of particulate matter suspension events in Iceland. *J. Aerosol. Sci.* 128, 99–113. doi: 10.1016/j.jaerosci.2018.12.004

Carlsen, H. K., Gislason, T., Forsberg, B., Meister, K., Thorsteinsson, T., Jóhannsson, T., et al. (2015). Emergency hospital visits in association with volcanic ash, dust storms and other sources of ambient particles: a time-series study in Reykjavik, Iceland. *Int. J. Environ. Res. Public Health* 12, 4047–4059. doi: 10.3390/ijerph120404047

Cas, R. A. F., and Wright, J. V. (1987). *Volcanic Successions: Modern and Ancient: A Geological Approach to Processes, Products and Successions*. Crows Nest, QLD: Allen & Unwin, doi: 10.1007/978-0-412-44640-5

Collini, E., Osores, M. S., Folch, A., Viramonte, J. G., Villarosa, G., and Salmuni, G. (2013). Volcanic ash forecast during the June 2011 Cordón Caulle eruption. *Nat. Hazards* 66, 389–412. doi: 10.1007/s11069-012-0492-y

Craig, H. M., Wilson, T. M., Stewart, C., Outes, V., Villarosa, G., and Baxter, P. J. (2016). Impacts to agriculture and critical infrastructure in Argentina after ashfall from the 2011 eruption of the Cordón Caulle volcanic complex: an assessment of published damage and function thresholds. *J. Appl. Volcanol.* 5:7. doi: 10.1186/s13617-016-0046-1

Del Bello, E., Taddeucci, J., Merrison, J. P., Alois, S., Iversen, J. J., and Scarlato, P. (2018). Experimental simulations of volcanic ash resuspension by wind under the effects of atmospheric humidity. *Sci. Rep.* 8:14509. doi: 10.1038/s41598-018-32807-2

Douillet, G. A., Rasmussen, K. R., Kueppers, U., Lo Castro, D., Merrison, J. P., Iversen, J. J., et al. (2014). Saltation threshold for pyroclasts at various bedslopes: wind tunnel measurements. *J. Volcanol. Geotherm. Res.* 27, 14–24. doi: 10.1016/j.jvolgeores.2014.03.011

Edwards, P., Varela, S. A., López, D. R., Willems, P. M., López, A. S., and Gyenge, J. E. (2017). Evidence on the response of Patagonian forage grasses to the mulching effect of recent tephra deposits in Argentina. *Arid L. Res. Manag.* 0, 1–15. doi: 10.1080/15324982.2017.1349209

Elissondo, M., Baumann, V., Bonadonna, C., Pistolesi, M., Cioni, R., Bertagnini, A., et al. (2016). Chronology and impact of the 2011 Cordon Caulle eruption, Chile. *Nat. Hazards Earth Syst. Sci.* 16, 675–704. doi: 10.5194/nhess-16-675-2016

Fernández-Arhex, V., Buteler, M., Amadio, M. E., Enriquez, A., Pietrantuono, A. L., Stadler, T., et al. (2013). The effects of Volcanic Ash from Puyehue-Caulle Range Eruption on the Survival of Dichroplus vittigerum (Orthoptera: Acrididae). *Florida Entomol.* 96, 286–288. doi: 10.1653/024.096.0149

Fisher, V. R., and Schmincke, H. U. (1984). *Pyroclastic Rocks*. Berlin: Springer-Verlag.

Folch, A., Mingari, L., Osores, M. S., and Collini, E. (2014). Modeling volcanic ash resuspension – application to the 14–18 October 2011 outbreak episode in central Patagonia, Argentina. *Nat. Hazards Earth Syst. Sci.* 14, 119–133. doi: 10.5194/nhess-14-119-2014

Forte, P., Domínguez, L., Bonadonna, C., Gregg, C. E., Bran, D., Bird, D., et al. (2018). Ash resuspension related to the 2011-2012 Cordón Caulle eruption, Chile, in a rural community of Patagonia, Argentina. *J. Volcanol. Geotherm. Res.* 350, 18–32. doi: 10.1016/j.jvolgeores.2017.11.021

Gaitán, J. J., Ayesa, J. A., Umaña, F., Raffo, F., and Bran, D. B. (2011). *Cartografía del área afectada por cenizas volcánicas en las provincias de Río Negro y Neuquén*. Available at: http://inta.gob.ar/documentos/cartografia-del-areaafectada-por-cenizas-volcanicas-en-las-provinciasde-rio-negro-y-neuquen/ (accessed December 12, 2012).

Global Volcanism Program, (2013). *Puyehue-Cordon Caulle (357150) in Volcanoes of the World, v. 4.8.4*, ed. E. Venzke (Washington, DC: Smithsonian Institution Offices).

Godagnone, R., and Bran, D. E. (2009). *Inventario Integrado de los Recursos Naturales de la Provincia de Río Negro. Geología, Hidrogeología, Geomorfología, Suelos, Clima, Vegetación y Fauna*. Río Negro: Instituto Nacional de Tecnología Agropecuaria.

Hadley, D., Hufford, G. L., and Simpson, J. J. (2004). Resuspension of Relic Volcanic Ash and Dust from Katmai: still an Aviation Hazard. *Am. Meteorol. Soc.* 19, 829–840. doi: 10.1175/1520-0434(2004)019<0829:rorvaa>2.0.co;2

Hincks, T. K., Aspinall, W. P., Baxter, P. J., Searl, A., Sparks, R. S. J., and Woo, G. (2006). Long term exposure to respirable volcanic ash on Montserrat: a time series simulation. *Bull. Volcanol.* 68, 266–284. doi: 10.1007/s00445-005-0006-9

Hobbs, P. V., Heggs, D. A., and Radke, L. F. (1983). Resuspension of volcanic ash from Mount St. Helens. *J. Geophys. Res.* 88, 3919–3921. doi: 10.1029/JC088iC06p03919

ICAO, (2007). *Meteorological Service or International Air Navigation Catalogue. Annex 3 to the Convention on International Civil Aviation*, 16th Edn. Montreal: ICAO.

Inman, D. L. (1952). Measures for describing the size distribution of sediments. *J. Sediment Pet.* 22, 125–145.

Jenkins, S. F., Wilson, T. M., Magill, C., Miller, V., Stewart, C., Marzocchi, W., et al. (2015). *Volcanic ash fall hazard and risk, UNISDR 2015 Global Assessment Report on Disaster Risk Reduction Technical Background Paper*. Geneva: United Nations Office for Disaster Risk Reduction (UNDRR).

Kok, J. F., Parteli, E. J. R., Michaels, T. I., and Karam, D. B. (2012). The physics of wind-blown sand and dust. *Reports Prog. Phys.* 75:106901. doi: 10.1088/0034-4885/75/10/106901

Langmann, B. (2013). Volcanic Ash versus Mineral Dust: atmospheric processing and environmental and climate impacts. *ISRN Atmos. Sci.* 2013, 1–17. doi: 10.1155/2013/245076

Leadbetter, S. J., Hort, M. C., Von Lwis, S., Weber, K., and Witham, C. S. (2012). Modeling the resuspension of ash deposited during the eruption of Eyjafjallajökull in spring 2010. *J. Geophys. Res. Atmos.* 117, 1–13. doi: 10.1029/2011JD016802

Liu, E. J., Cashman, K. V., Beckett, F. M., Witham, C. S., Leadbetter, S. J., Hort, M. C., et al. (2014). Ash mists and brown snow: remobilization of volcanic ash from recent Icelandic eruptions. *J. Geophys. Res. Atmos.* 119, 1–18. doi: 10.1002/2014JD021598.Received

Liu, E. J., Cashman, K. V., and Rust, A. C. (2015). Optimising shape analysis to quantify volcanic ash morphology. *GeoResJ* 8, 14–30. doi: 10.1016/j.grj.2015.09.001

Mcphie, J., Doyle, M., and Allen, R. (1993). *Volcanic Textures : A Guide to the Interpretation of Textures in Volcanic Rocks*. Hobart, TAS: University of Tasmania.

Mingari, L. A., Collini, E. A., Folch, A., Báez, W., Bustos, E., Osores, M. S., et al. (2017). Numerical simulations of windblown dust over complex terrain: the Fiambalá basin episode in June 2015. *Atmos. Chem. Phys.* 17, 6759–6778. doi: 10.5194/acp-17-6759-2017

Miwa, T., Nagai, M., and Kawaguchi, R. (2018). Resuspension of ash after the 2014 phreatic eruption at Ontake volcano, Japan. *J. Volcanol. Geotherm. Res.* 351, 105–114. doi: 10.1016/j.jvolgeores.2018.01.003

Panebianco, J. E., Mendez, M. J., Buschiazzo, D. E., Bran, D., and Gaitán, J. J. (2017). Dynamics of volcanic ash remobilisation by wind through the Patagonian steppe after the eruption of Cordón Caulle, 2011. *Sci. Rep.* 7:45529. doi: 10.1038/srep45529

Pistolesi, M., Cioni, R., Bonadonna, C., Elissondo, M., Baumann, V., Bertagnini, A., et al. (2015). Complex dynamics of small-moderate volcanic events: the example of the 2011 rhyolitic Cordón Caulle eruption, Chile. *Bull. Volcanol.* 77:3. doi: 10.1007/s00445-014-0898-3

Pye, K. (1987). *Aeolian dUst and Dust Deposits*. London: Academic Press.

Reckziegel, F., Bustos, E., Mingari, L., Báez, W., Villarosa, G., Folch, A., et al. (2016). Forecasting volcanic ash dispersal and coeval resuspension during the

April-May 2015 Calbuco eruption. *J. Volcanol. Geotherm. Res.* 321, 44–57. doi: 10.1016/j.jvolgeores.2016.04.033

Shao, Y. (2008). "Land-Surface Modelling," in *Physics and Modelling of Wind Erosion. Atmospheric and Oceanographic Sciences Library*, ed. Y Shao. Vol 37. Dordrecht: Springer.

Shao, Y., and Lu, H. (2000). A simple expression for wind erosion threshold friction velocity. *J. Geophys. Res.* 105, 22437–22443 doi: 10.1029/2000jd900304

Thorsteinsson, T., Jóhannsson, T., Stohl, A., and Kristiansen, N. I. (2012). High levels of particulate matter in Iceland due to direct ash emissions by the Eyjafjallajkull eruption and resuspension of deposited ash. *J. Geophys. Res. Solid Earth* 117, 1–9. doi: 10.1029/2011JB008756

Újvári, G., Kok, J. F., Varga, G., and Kovács, J. (2016). The physics of wind-blown loess: implications for grain size proxy interpretations in Quaternary paleoclimate studies. *Earth Sci. Rev.* 154, 247–278. doi: 10.1016/j.earscirev.2016.01.006

Ulke, A. G., Torres Brizuela, M., Raga, G. B., and Baumgardner, D. (2016). Aerosol properties and meteorological conditions in the city of Buenos Aires, Argentina, during the resuspension of volcanic ash from the Puyehue-Cordón Caulle eruption. *Nat. Hazards Earth Syst. Sci.* 16, 2159–2175. doi: 10.5194/nhess-16-2159-2016

UNEP, WMO, and UNCCD, (2016). *Global Assessment of Sand and Dust Storms*. Nairobi: United Nations Environment Programme.

Wilson, T., Stewart, C., Bickerton, H., Baxter, P., Outes, V., Villarosa, G., et al. (2013). Impacts of the June 2011 Puyehue-Cordón Caulle volcanic complex eruption on urban infrastructure, agriculture and public health. *GNS Sci.* 20, 1–88.

Wilson, T. M., Cole, J. W., Stewart, C., Cronin, S. J., and Johnston, D. M. (2011). Ash storms: impacts of wind-remobilised volcanic ash on rural communities and agriculture following the 1991 Hudson eruption, southern Patagonia, Chile. *Bull. Volcanol.* 73, 223–239. doi: 10.1007/s00445-010-0396-1

WMO, (1975). *International Cloud Atlas. Manual on the Observation of Clouds and Other Meteors*. Geneva: WMO.

Conflict of Interest: The authors declare that the research was conducted in the absence of any commercial or financial relationships that could be construed as a potential conflict of interest.